Quaternary Science Reviews 131 (2016) 193–210

Contents lists available at ScienceDirect

Quaternary Science Reviews

journal homepage: www.elsevier.com/locate/quascirev

Holocene paleoclimate history of Fallen Leaf Lake, CA., from geochemistry and sedimentology of well-dated sediment cores

Paula J. Noble [a, *], G.Ian Ball [b], Susan H. Zimmerman [c], Jillian Maloney [d], Shane B. Smith [a], Graham Kent [e, g], Kenneth D. Adams [f], Robert E. Karlin [a], Neil Driscoll [g]

[a] Department of Geological Sciences and Engineering, University of Nevada, Reno, NV 89557, USA
[b] Chevron Energy Technology Company, 1500 Louisiana Street, Houston, TX 77002, USA
[c] Center for Accelerator Mass Spectrometry, Lawrence Livermore National Laboratory, Livermore, CA 94550, USA
[d] Department of Geological Sciences, San Diego State University, San Diego, CA 92182, USA
[e] Nevada Seismological Laboratory, University of Nevada, Reno, NV 89557, USA
[f] Division of Earth and Ecosystem Sciences, Desert Research Institute, Reno, NV 89512, USA
[g] Scripps Institute of Oceanography, Geosciences Research Division, La Jolla, CA 92093, USA

ARTICLE INFO

Article history:
Received 8 June 2015
Received in revised form
19 October 2015
Accepted 23 October 2015
Available online xxx

Keywords:
Holocene
Lake cores
Geochemistry
Paleoclimate
Lake Tahoe basin
Great Basin
Neopluvial

ABSTRACT

Millennial-scale shifts in aridity patterns have been documented during the Holocene in the western United States, yet the precise timing, severity, and regional extent of these shifts prompts further study. We present lake sediment core data from Fallen Leaf Lake, a subalpine system at the southern end of the Lake Tahoe basin for which 80% of the contemporary inflow is derived from snowpack delivered by Pacific frontal storm systems. A high quality age model has been constructed using ^{14}C ages on plant macrofossils, ^{210}Pb, and the Tsoyowata tephra datum (7.74–7.95 cal kyr BP). One core captures the transition from the Late Tioga-younger Dryas glaciolacustrine package to laminated opaline clay at 11.48 cal kyr BP. Early Holocene sedimentation rates are relatively high (~1.9 mm/year) and cooler winter temperatures are inferred by the presence of pebbles interpreted to be transported out into the lake via shore ice. There is a geochemically distinct interval from ~4.71 to 3.65 cal kyr BP that is interpreted as a late Holocene neopluvial, characterized by depleted $\delta^{13}C$ and lower C:N that point to reduced runoff of terrigenous organic matter, increased winter precipitation, and increased algal productivity. The largest Holocene signal in the cores occurs at the end of the neopluvial, at 3.65 cal kyr BP, and marks a shift into a climate state with variable precipitation, yet is overall more arid than the neopluvial. This new climate state persists for ~3 ka, until the Little Ice Age. Low sedimentation rates (0.5 mm/year), the homogeneous opaline sediment, and steadily increasing contributions of terrestrial vs. algal organic matter in these cores suggest that the lowstand state of Fallen Leaf Lake may have been the norm from 3.65 to 0.55 cal kyr BP, punctuated by short term high precipitation years or multi-year intervals capable of rapid short duration lake level rise. Fallen Leaf Lake is strongly influenced by changes in winter precipitation and temperature, manifested largely by the geochemical proxies, and highlights unique advantages of subalpine lakes in regional paleoclimate reconstructions.

1. Introduction

Here we characterize the Holocene sedimentary package of a glacially derived subalpine lake in the Lake Tahoe basin to better constrain the timing and nature of major paleoclimatic shifts in the northern Sierra Nevada and western margin of the Great Basin over the last ~13 ka. Fallen Leaf Lake (FLL) is a hydrologically open oligotrophic subalpine system situated at the southern margin of Lake Tahoe. Presently, the basin experiences a typical montane Sierra Nevada climate dominated by Pacific frontal storm systems bringing precipitation largely in the winter (Hanes, 1981; O'Hara, 2007), however the intensity and position of synoptic scale climate patterns may have varied throughout the Holocene (Barron and Anderson, 2011), contributing to significantly different annual

* Corresponding author.
E-mail address: noblepj@unr.edu (P.J. Noble).

http://dx.doi.org/10.1016/j.quascirev.2015.10.037
0277-3791/

precipitation patterns. Most Holocene climate reconstructions for the Sierra Nevada and western Great Basin have been derived from the alkaline terminal lakes of endorheic basins (e.g., Pyramid, Owens, Mono, Walker lakes) whereas relatively few have come from higher elevation and potentially more climatically sensitive alpine environments (Osleger et al., 2009; Smith et al., 2013; Street et al., 2012, 2013). Alkaline terminal lakes produce endogenic carbonates particularly suited to $\delta^{18}O$ analysis and reconstruction of basin-scale water budgets governed by past changes in the relative magnitudes of precipitation and evaporation. However, the lack of macrofossils and variable and unknown reservoir effects on carbonates in these endorheic systems has complicated the construction of age-models used as a basis for interpreting the timing and periodicity of the climatic events. In contrast, subalpine lakes may offer higher fidelity records of past climatic change. They are usually rich in macrofossils that can be ^{14}C-dated, enabling the creation of reliable high-resolution age models, and their low drainage-area to lake-surface ratio should be more responsive to hydrologic cycle perturbations. Climatic effects relating to the strength and degree of winter precipitation can also have discernible effects on subalpine lake productivity and its organic geochemical record, resulting from changes in amounts of lake mixing and the development of stratification. This study provides an opportunity to identify and calibrate the subalpine response to major climate signals affecting the northern Sierra Nevada and western Great Basin, and to inform the timing of regional climate events using a high-resolution age model.

2. Setting and previous work on FLL sediments

Fallen Leaf Lake (FLL) is a low conductivity, circumneutral (pH = 6.5–7.5) deep subalpine lake situated ~2 km south of Lake Tahoe in Glen Alpine Valley at an elevation of 1942 m, 45 m above Lake Tahoe (Fig. 1). The northern end is bounded by terminal moraines left during the retreat of Tioga-, and possible Tahoe-age glaciers (Saucedo et al., 2005).

The southwestern margin of FLL is bounded by the steep escarpment of the West Tahoe-Dollar Point fault (Brothers et al., 2009). The principal source of water and sediment inflow is Glen Alpine Creek on the southern end of the lake. Outflow is at the north end through Taylor Creek and subsurface flow through the end moraine into Lake Tahoe (Fig. 1; Kleppe et al., 2011). The watershed for FLL is ~42 km^2 of steep montane areas in the Desolation Wilderness, and is ~8 times the surface area of FLL (Kleppe, 2005). Mean annual precipitation in the watershed ranges from 0.75 m to 1.5 m, the majority of which falls in the winter as snow (Hanes, 1981). Lake levels have been observed to rise quickly following periods of high precipitation, and have been inferred to drop to the level of Tahoe during prolonged drought periods, including a lowstand during the Medieval Climate Anomaly circa 1.0–0.7 cal kyr BP (Kleppe et al., 2011; Mann et al., 2009). Bathymetric profiles show that the lake is crossed by a series of recessional moraines that divide the lake into northern and southern sub-basins. The deepest end of the lake is to the south with a maximum depth of 116 m (Maloney et al., 2013), and the northern end is filled with a series of moraine ridges averaging about 70 m depth.

Side scan sonar, Compressed High Intensity Radar Pulse (CHIRP) surveys, and a piston coring campaign were conducted in 2006 to assist with reconstructing the frequency and origins of past earthquakes in the Lake Tahoe Basin (Brothers et al., 2009; Maloney et al., 2013). This previous subsurface imaging delimited gross sedimentologic packages and enabled identification of suitable locations for a subsequent 2010 coring campaign that sought to capture a paleoclimate record by recovering cores that preserved

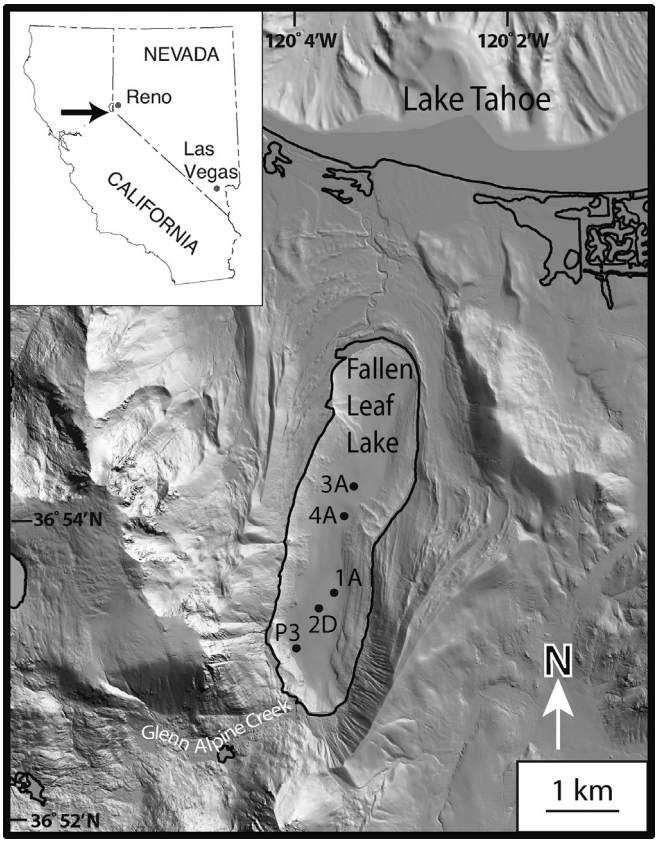

Fig. 1. Digital elevation map showing the location of Fallen Leaf Lake in the southern part of the Lake Tahoe basin, and core localities.

the upper ~1 m of sediments. The upper ~1 m was not recovered in the 2006 coring campaign because of over-penetration. The 2006 cores were proximally positioned to the West Tahoe-Dollar Point Fault and captured debris and gravity driven flows, including one ascribed to the most recent seismic event (FLLS1). One core also captured the Tsoyowata tephra that, along with sparse macrofossil ^{14}C dating provided a rough portrait of the sedimentologic character, sedimentation rates, and distribution of datable macrofossils in FLL.

The piston cores collected in 2010 were also used to constrain the ages of debris and gravity-driven deposits observed in CHIRP data. It was hypothesized that these flows were triggered by seismic events and, as such, were used to expand the paleoseismic history of the West Tahoe-Dollar Point Fault (Maloney et al., 2013). Radiocarbon dates from these cores were presented in Maloney et al. (2013), although in the context of the paleoseismological history. The major seismic events dated by this effort are termed FLLS1 (4.71 ± 0.14 cal kyr BP), FLLS2 (7.75 ± 0.14 cal kyr BP), and FLLS3 (11.48 ± 0.17 cal kyr BP), and are represented in the piston cores by turbidite deposits that act as marker beds to correlate stratigraphy between cores and CHIRP data (Maloney et al., 2013).

3. Materials and methods

3.1. Coring

Four coring sites were targeted based on previous seismic surveys (Brothers et al., 2009; Maloney et al., 2013), two in the northern sub-basin, and two in the southern (Fig. 1). Piston and accompanying gravity cores were taken in 2010 using the

Kullenberg piston coring system by staff from the Limnological Research Center (LRC), University of Minnesota. The first site in the southern sub-basin (core 1A; 9.84 m length) is at 115 m water depth in a moat on the eastern flank of the basin, where seismic units thin into a more condensed section that allowed for greater stratigraphic penetration (Fig. 2). A second site in the southern sub-basin (cores 2D; 11.5 m length, 2E; 0.44 m length) is at 111 m water depth where the sediment is thickest and forms a slight bulge in the basin center. In the northern sub-basin, two sites were cored, each situated between morainal ridges in pockets of Holocene sedimentary fill. Site 4 (core 4A; 4.45 m length), at 98.5 m water depth occurs just north of the first morainal ridge that divides the two sub-basins, and site 3 (cores 3A; 4.6 m length, 3B; 0.44 m length) is the furthest north at 94.9 m water depth. Cores were shipped to the LRC core facility in Minneapolis for processing and sampling, and are archived at the National Lacustrine Core Repository at the University of Minnesota under the project identifier BOLLY-FLL10 (Table 1).

3.2. Core processing, sampling, and geochemical analyses

Cores were split, logged and imaged, and high resolution magnetic susceptibility was measured using a GEOTEK multi-sensor core logger every 5 mm. Samples were taken for organic geochemical analysis every 8–10 cm throughout core 2D, which has the highest sediment accumulation rates and is the most stratigraphically complete. Additional organic geochemistry samples were taken from the base of core 1A to provide data from the oldest cored interval, and also from the upper 3 m of the northernmost core (3A) to provide a comparison between sites during the last 7 ka. Core 3A was sampled roughly every 4 cm because it is more condensed, with the upper 3 m representing the last 7 ka. All core depths are reported as centimeters below lake floor.

Archived halves underwent X-ray fluorescence (XRF) analysis at the Large Lake Observatory in Duluth, MN using an ITRAX core scanner. Samples were run using a Mo source at 2 mm intervals with a 30s dwell time. Initial data reduction and analysis of XRF data was conducted in R version 2.15.0 (R Core Team, 2012) using the rda function in the package 'vegan' version 2.0–6 (Oksanen et al., 2013) to run principal component analysis on major elements. Stratigraphic plots of XRF data were constructed in C2 version 1.5 (Juggins, 2007). XRF data are reported as unprocessed intensities (i.e. counts) for single elements and log-ratios on normalized counts. The log-ratios have been demonstrated to provide a more linear relationship between element intensity and element concentration (Weltje and Tjallingii, 2008) and are thus used on the normalized data. Opal analyses were performed on one of the older cores, 06-P3, in 2009 using a modified method of silica extraction, as outlined in Mortlock and Froelich (1989) and Calvert et al. (2001).

Sediment samples were processed and analyzed for TOC (%), TN (%), $\delta^{13}C$, and $\delta^{15}N$ at the Nevada Stable Isotope Lab at UNR. The $\delta^{13}C$ and $\delta^{15}N$ values are reported relative to PeeDee Belemnite (PDB) and air, respectively. Subsamples (~1 g wet sediment) were bathed in HCl fumes overnight to remove any carbonates, dried at 60 °C for ~48 h, ground to a homogenous powder, and ~25–35 mg sediment (dry weight) was packed into tins and analyzed by elemental

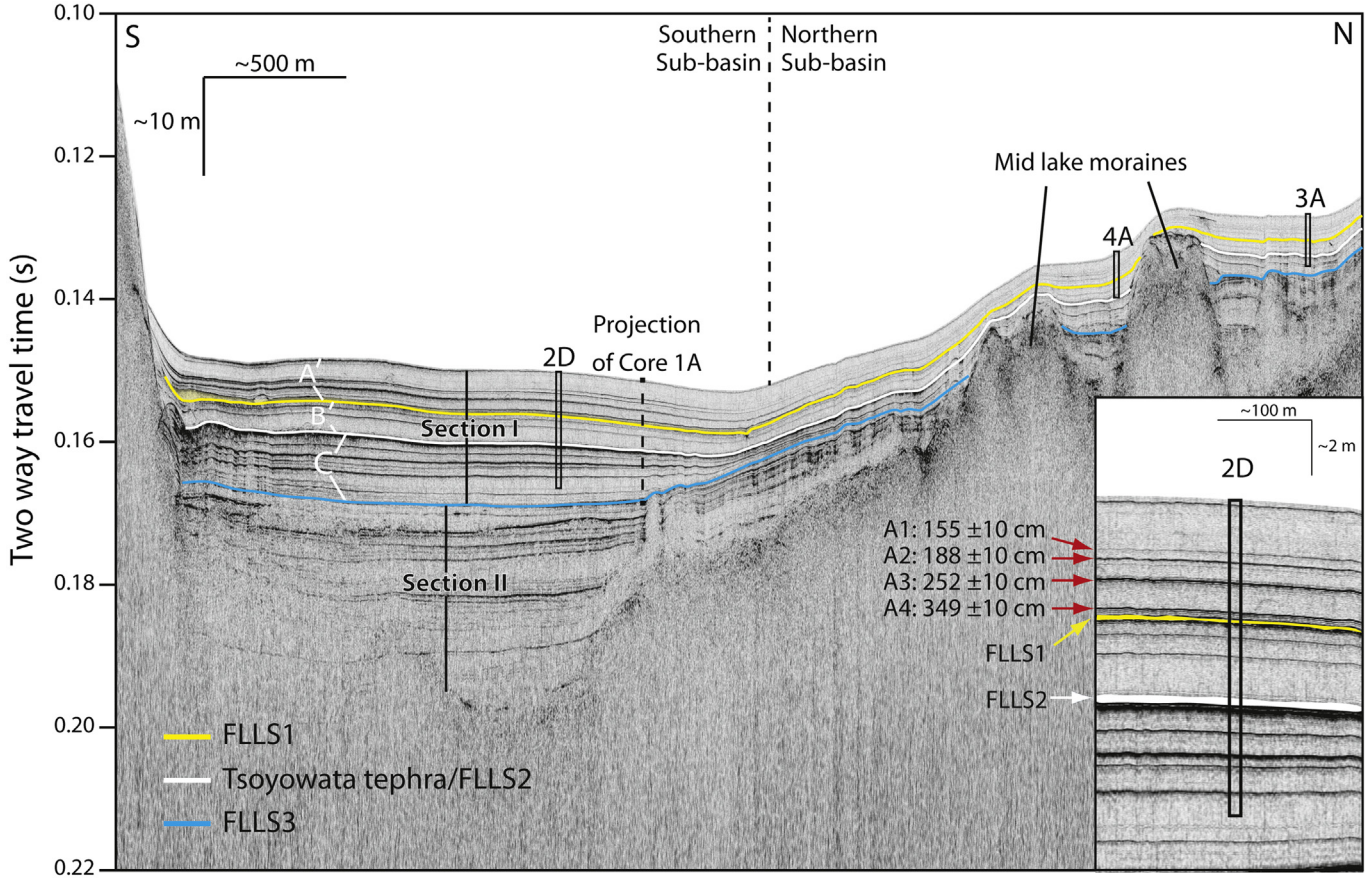

Fig. 2. Longitudinal North-South CHIRP profile through FLL showing position of cores 2D, 3A, and 4A and the projection of core 1A onto this line. Stratigraphic packages and marker horizons are labeled. Inset on lower right is a magnification of the upper part of the core 2D site showing reflectors A1 through A4 that are discussed in the text.

Table 1
Metadata for 2010 piston and gravity cores.

Site & hole	Hole ID	Core type	Core length (m)	Sediment length (m)	Water depth (m)	Latitude (°)	Longitude (°)
1A	BOLLY-FLL10-1A	Piston core	9.84	9.74	115.0	38.89344	−120.06313
2D	BOLLY-FLL10-2D	Piston core	11.54	11.32	111.0	38.89194	−120.06578
2E	BOLLY-FLL10-2E	Gravity core	0.52	0.42	111.0	38.89194	−120.06578
3A	BOLLY-FLL10-3A	Piston core	4.62	4.6	94.9	38.90551	−120.05973
3B	BOLLY-FLL10-3B	Gravity core	0.5	0.42	94.9	38.90551	−120.05973
4A	BOLLY-FLL10-4A	Piston core	4.45	3.93	98.5	38.90209	−120.06145

analysis isotope ratio mass spectrometry (EA-IRMS). No visible plant debris was present in any of the prepared sediment samples. Standards (acetanilide) of known elemental and isotopic composition, and of known masses, were interspersed every 10–15 samples. The diatom-rich sediment was extremely hygroscopic and, as such, samples were always weighed immediately after drying. Reproducibilities, as determined from replicate sample analyses, were: for TOC ±0.03% (1σ), TON < ±0.01% (1σ), $\delta^{13}C$ ± 0.04‰ (1σ), and for $\delta^{15}N$ ± 0.15‰ (1σ). Fifteen samples, plus five replicates, were analyzed from sections 7 and 8 of core 1A, representing a 20 cm sampling resolution. 130 samples, and 22 replicates were analyzed from all sections (1–8) of core 2D, or every 8–12 cm. 36 samples and 6 replicates were analyzed from Section 1 of core 3A, or about every 4 cm. 214 measurements were made in total corresponding to 181 depth measurements for $\delta^{13}C$, $\delta^{15}N$, TOC, and TN across the three cores.

3.3. Core chronology; ^{210}Pb, radiocarbon and tephrochronology

Gravity cores from sites 2 and 3 (cores 2E and 3B, respectively) were sectioned and processed for ^{210}Pb dating. Based on an initial sediment accumulation rate estimate of ≤2 mm/year, the top 35 cm of core 2E and the top 27 cm of core 2B were sectioned at 0.5 cm intervals and the remainder was sectioned every 1 cm thereafter. As a preliminary processing step, loss on ignition (LOI) was conducted at the LRC in Minneapolis following their standard operating procedure based on Dean (1974), and ^{210}Pb dating was conducted at the Harmon Research Center, St. Croix Watershed Research Station in Minnesota.

Organic macrofossils (n = 42) from the cores consist mostly of pine needles, leaves, and bark fragments, and were analyzed for their radiocarbon content at the Center for Accelerator Mass Spectrometry at Lawrence Livermore National Laboratory (Table 2). Age models were created for each piston core using a Poisson-process deposition model in OxCal v. 4.1.7 (Bronk Ramsey, 2009) that allows for fluctuations in deposition rate. The IntCal04 calibration curve (Reimer et al., 2004) was used in the Oxcal models, and ages were interpreted to 2σ uncertainties. Composite age models were generated for two depositional events.

Lastly, the Tsoyowata tephra, named and first documented in the Tahoe region by Davis (1978), is a valuable chronostratigraphic marker in some of the cores. The age of this tephra is 7015 ± 45 ^{14}C yr BP (7.74–7.95 cal kyr BP) as reported in Bacon (1983), and was added into the age model.

4. Results and discussion

4.1. Chronology

^{210}Pb age models (Fig. 3) provide a determination of sediment accumulation rates in both gravity cores over the past 200 years, and constrain the age of the uppermost few centimeters of lake floor sediment. The gravity cores are currently being used for additional high-resolution studies into the last millennium (Engstrom et al., 2014; Johnson, 2013). Both gravity cores show consistent patterns in sediment accumulation, the most notable being an increase starting in the 1950's, which is associated with anthropogenic activities around the lake (Johnson, 2013). There is a stark difference in sedimentation rate between the two cores. Core 2E from the southern sub-basin, closer to the inflow point from Glen Alpine Creek, has a rate that is roughly 3 times higher than core 3B from the northern sub-basin (Fig 3). Core 2E ^{210}Pb ages were also incorporated into the Oxcal model of the accompanying 2D piston core to improve age constraints on the upper 50 cm of the piston core.

Radiocarbon ages for each of the FLL10 cores are presented in Table 2, and age models for each core are found in Fig. 4. Event models run for FLLS1, 2, and 3 are discussed in Maloney et al. (2013), and the age model for the FLL06-P3 core is presented in Brothers et al. (2009). Of the 42 ^{14}C ages acquired on the 2010 core suite, only one was thrown out (BOLLY-3A1-150) from the models because it was anomalously old, dated as 26.83 ± 0.16 cal kyr ^{14}C BP (Table 2). Core 2D, with 15 ^{14}C ages produced the best age model and the top of the core was further constrained using the ^{210}Pb results from its companion gravity core (2E). Uncertainties for most of the middle and late Holocene, above the Tsoyawata ash, are comparatively small, ranging from ±80 to as low as ±45 years. Uncertainties from the early Holocene, below the Tsyowata ash, are slightly larger (±100 years) and increase steadily to ±388 years at the base of the core. Mean uncertainty is ±141 years. The uncertainties for core 1A, 3A, 4A are generally ±100 years or higher with mean uncertainties of ±255 years in 1A, ±366 years 3A, and ±149 years in core 4A.

4.2. Sedimentology and stratigraphy

FLL sediment is dominated by olive to dark gray opaline clay with homogeneous, laminated, and mottled textures, and occasional dark or yellow bands. Siliciclastic beds, including some that have been interpreted as seismically-induced turbidites and slide deposits (Brothers et al., 2009; Smith et al., 2013), make up a subordinate component in the 2010 cores (Fig. 5). Opal content, run on FLL10-P3 (Fig. 6), ranges from 29 to 72% (weight) in the non-clastic background sediment, and from 6 to 53% in bands and siliciclastic beds.

Magnetic susceptibility values range from near zero to >200 × 10^{-6} SI (Systeme International units). High values in magnetic susceptibility are driven largely by clastic input in the glaciolacustrine interval and in turbidites. The shape of the magnetic susceptibility peaks in the turbidites is characteristically asymmetrical with the peak near the base and gradually decreasing towards the top. Baseline values for magnetic susceptibility in the sedimentary intervals between turbidites is very low, varying from <1–15 × 10^{-6} SI. There is a subtle difference in baseline magnetic susceptibility values between the northern and southern sub-basins. Magnetic susceptibility baseline values are <1 × 10^{-6} SI in the south and 2–5 × 10^{-6} SI in the north, reflective of both a lower sediment accumulation rate and a higher detrital fraction in the north.

Table 2
^{14}C ages from 2010 core suite, cmblf = cm below lake floor.

CAMS#	Sample name	Sample description	Depth (cmblf)	^{14}C age (years BP)	±	Calibrated age (cal BP)	± (1σ)	± (2σ)
152537	BOLLY-1A1-53	Pine needles	48	2020	30	1971	42	84
152538	BOLLY-1A1-77	Small leaf	72	2170	90	2167	112	224
152541	BOLLY-1A1-120	Pine needle	115	2485	30	2576	85	170
152539	BOLLY-1A1-121	Pine needle	116	2480	30	2572	88	176
152540	BOLLY-1A3-12.5	Pine needle	176	3095	35	3313	44	88
152695	Bolly-1A3-65	Twig	228.5	3735	30	4101	60	119
152542	BOLLY-1A5-22	Connifer cone seed	410.5	4515	45	5166	87	174
152696	Bolly-1A5-142	Wood or pine needle fragment	529	6165	30	7069	47	95
152543	BOLLY-1A6-149	Pine needle	686	8045	40	8917	87	174
152544	BOLLY-1A7-5.5	Pine needle	693.5	8190	45	9148	78	156
152545	BOLLY-1A8-55	Twig	894	10335	35	12184	100	200
152719	Bolly-1A8-76	Unspecif. organic fragments	915	10540	35	12547	78	155
152697	Bolly-1A8-111	Unspecif. organic fragments	950.5	11460	60	13316	55	110
152546	BOLLY-1A8-cc	Unspecif. organic fragments	987	11070	90	13001	75	150
152547	BOLLY-2D1-54	Pine needle	41.5	765	30	698	19	38
160609	BOLLY-2D1 91	Pine needle	78.5	1480	40	1370	44	88
152548	BOLLY-2D1-117	Deciduous leaf	104.5	1880	30	1819	45	90
152684	Bolly-2D1-138.5	Pine needle fragment	126.5	2175	40	2192	66	132
152685	Bolly-2D2-38	Pine needle fragment	165	3000	80	3167	103	207
152686	Bolly-2D2-48	Pine needle fragment	175	3090	35	3299	41	82
160610	BOLLY-2D2 48.5	Pine needle	175.5	3105	40	3322	49	98
152687	Bolly-2D3-25	Deciduous leaf	302	4110	30	4668	73	146
152688	Bolly-2D3-46	Pine needle	323	4120	30	4671	72	144
152689	Bolly-2D4-28	Degraded pine needle	431	4630	40	5430	70	140
152698	Bolly-2D4-53	Pine needle fragment	466	4910	40	5654	33	66
152699	Bolly-2D4-88	Pine needle	501	5250	30	6051	63	127
152700	Bolly-2D4-108	Pine needle	521	5300	30	6087	49	97
152701	Bolly-2D6-50.5	Wood-bark	645.5	6660	30	7531	26	52
152702	Bolly-2D6-77.5	Pine needle	672.5	6805	35	7636	25	51
152703	Bolly-2D8-7.5	Twig	838.5	7885	30	8768	89	177
152704	Bolly-2D9-123	Pine needle fragment	1105	9050	140	10152	208	415
152705	Bolly-3A1-60	Pine needle fragment	58.5	2060	35	2026	48	96
152706	Bolly-3A1-70	Pine needle	68.5	2130	30	2149	75	149
152707	Bolly-3A1-105.5	Pine needle	104	2750	35	2846	40	81
160608	BOLLY-3A1 107	Leaf fragment	105.5	2815	40	2921	56	112
152709	Bolly-3A2-66	Pine needle fragment	218.5	4980	45	5745	71	142
152710	Bolly-3A3-18.25	Pine needle	325	6640	35	7519	30	60
160611	BOLLY-4A1 79	Leaf fragment	66.5	895	50	821	59	118
160612	BOLLY-4A1 89.5	Bark	77	1215	40	1145	60	120
-	Bolly-4A1 89.5 combined	Bark	77			1101	47	94
160614	BOLLY-4A1 89.5 rep	Bark	77	1145	35	1061	59	118
160613	BOLLY-4A3 79.5	Unspecif. organic fragments	371	5880	90	6701	114	228
152690	Bolly-2E-43	Leaf and pine needle fragment	33	950	60	848	56	112
152691	Bolly-3B-8	Pine needle	1	200	30	149	77	154
152708	Bolly-3A1-150	Pine needle	150	26820	160	26826	160	320

Core stratigraphy can be divided into several stratigraphic packages based on lithologic breaks, distinctive marker beds, and magnetic susceptibility (Fig. 5). The major stratigraphic packages observed in core are 1.) the Pleistocene Late Tioga glaciolacustrine-Younger Dryas interval (Section II in CHIRP data), 2.) the early Holocene, pre-Tsoyowata interval (Section I, unit IC in CHIRP), 3.) the mid Holocene post Tsoyowata/FLLS2 interval (Section I, unit IB in CHIRP), and 4.) the late Holocene post FLLS1 interval (Section I, unit 1A in CHIRP). These packages can be traced within the lake basin on CHIRP data. Their acoustic character, geometry, and spatial distribution are discussed in Maloney et al. (2013) and shown in Fig. 2. Within unit 1A, several strong and traceable reflectors are observed, and in core 2D the depths and age of four of these reflectors, labeled A1 through A4, are indicated (Fig. 2). The physical properties, age, and depositional character of these units are further described below.

4.2.1. Late Tioga-Younger Dryas interval (13.93–11.48 cal kyr BP)

This interval corresponds to the top of Section II in the CHIRP profiles, and was recovered only in the lower 0.5 m of core 1A. The glaciolacustrine sediments, which are present in the lower 0.5 m of this interval, are composed of silty vivianite-bearing bluish gray clay with high magnetic susceptibility values that generally range between 100 and 150 $\times$ 10^{-6} SI. Above the silty glaciolacustrine sediments, this interval changes in character and consists of mm-scale laminations of olive yellow to dark olive silty opaline clay. Magnetic susceptibility steadily decreases throughout the laminated part of this interval from 60 $\times$ 10^{-6} SI to 5 $\times$ 10^{-6} SI at the top of the interval. The age model indicates that the base of the core is 13.93 ± 0.73 cal kyr BP and the top of this interval is 11.48 ± 0.17 cal kyr BP. The upper laminated part of this interval is roughly equivalent to the late Pleistocene Younger Dryas Chronozone (12.85–11.65 cal kyr BP). The glaciolacutrine-Younger Dryas interval is overlain by a 4.5 cm thick turbidite with a 1 cm sandy base (FLLS3; Maloney et al., 2013) that is interpreted to be generated by a seismic event at 11.48 cal kyr BP and permits correlation to the sediment sequences in Lake Tahoe, Emerald Bay, and Cascade Lake (Maloney et al., 2013; Smith et al., 2013).

4.2.2. Early Holocene pre-Tsoyowata interval (11.48–7.93 cal kyr BP)

This interval corresponds to Section I, unit 1C in CHIRP profiles and is observed in 3 of the cores (1A, 2D, 3A). The interval is characterized by faintly laminated dark gray to olive opaline clay. In

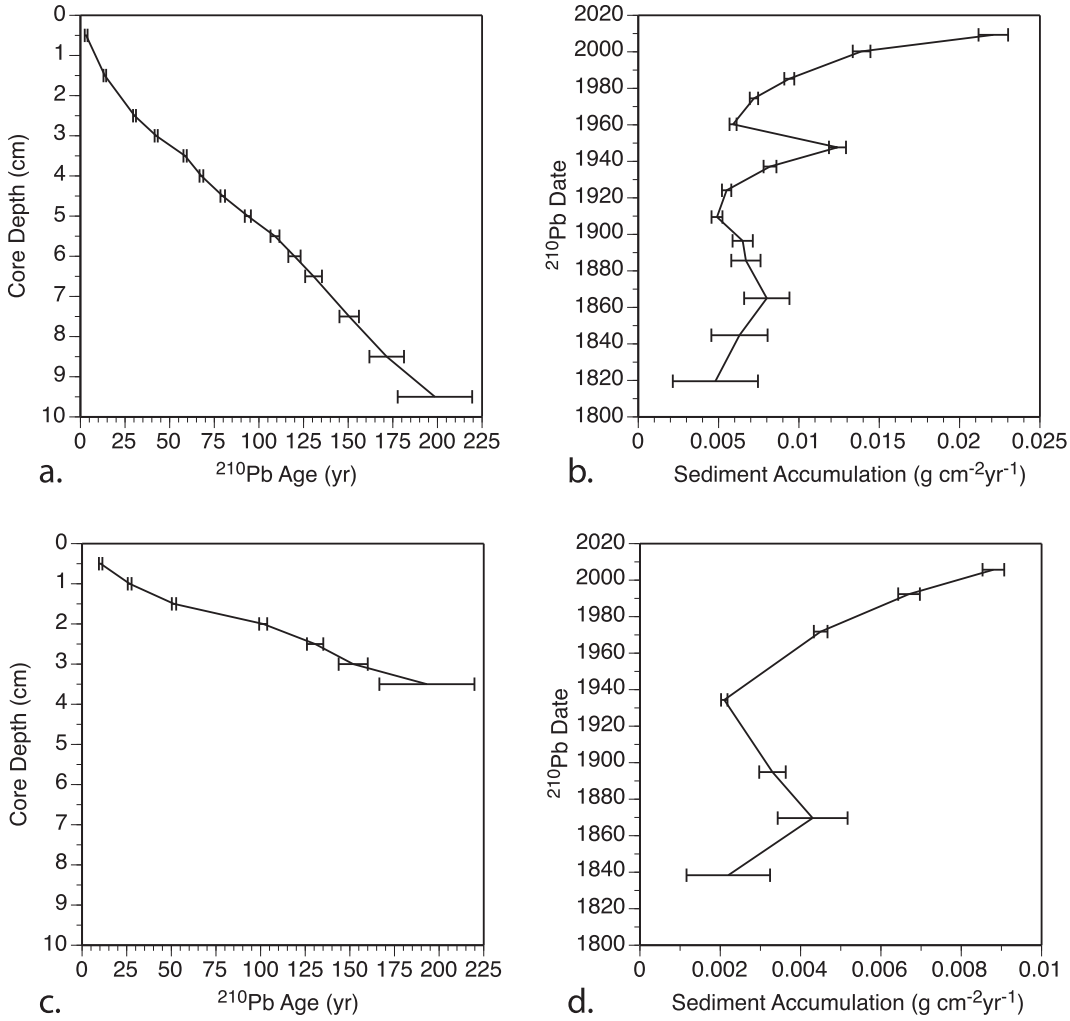

Fig. 3. 210 Pb age model and sediment accumulation rates for gravity cores. See Fig. 1 for location.

the southern sub-basin, the cores are an opaline clay with faint yellowish olive to darker olive laminations that become progressively disrupted and mottled upwards in the core. In the northern sub-basin (core 3A), this interval is characterized by a darker, discontinuously laminated to mottled opaline clay. In core 1A, there are 3 distal turbidite beds observed in this interval (at 747–751 cm, 695–699 cm, and 618–623 cm), consisting of 1–2 cm silty layers overlain by 1–2 cm of lighter gray clay, ranging from 2 to 5 cm thick, and accompanied by small magnetic susceptibility peaks ranging from 6 to 90 $\times$ 10^{-6} SI. Also present in this interval are scattered rocks that may be a result of ice rafting. The top of this unit is easily recognized by the Tsoyowata tephra.

4.2.3. Tsoyowata tephra and FLLS2 interval (7.93–7.75 cal kyr BP)

The Tsoyowata tephra was penetrated in all cores but 4A, which stopped roughly one half meter short, based on correlation using the CHIRP profiles. The Tsoyowata tephra is an airfall tephra that was sourced from Mount Mazama (Sarna-Wojcicki et al., 1991), and is also present in Lake Tahoe (Davis, 1978; Hyne et al., 1972; Smith et al., 2013). The tephra is a stiff white 3–4 cm thick layer overlain by a 1–3 cm thick layer of light gray diatomaceous ash-rich clay. The gray clay is in turn overlain by a distal turbidite, FLLS2 (Maloney et al., 2013) that, where best developed, consists of a basal 0.5 m of fine sand that grades into silty opaline clay, rich in organic debris. The top of the turbidite is clearly visible as a light gray clay layer that grades into the overlying opaline clay over several cm. In core 2D, the ash was disturbed during coring and is depicted as being a thicker interval in Fig. 5; in fact it is the same thickness in cores 1A and 2D. Unlike the ash, which is uniform in thickness throughout the lake, the turbidite appears to infill lows and thin to the north. It is 40 cm thick in core 1A, which lies in a moat in the southern sub basin, and is only 3 cm thick to the north in core 3A. CHIRP profiles show that FLLS2 is laterally continuous with slumps and debris flows imaged along the southwest margin of the lake in proximity to the West Tahoe Dollar Point fault, and is interpreted by Maloney et al. (2013) to be seismically triggered. FLLS2 is correlative to events recognized in Lake Tahoe, Emerald Bay, and Cascade Lake (Maloney et al., 2013; Smith et al., 2013). The age of FLLS2 is modeled as 7.75 $\pm$ 0.14 cal kyr BP using a composite of dates from three of the cores.

4.2.4. Mid-holocene post Tsoyowata interval (7.75–4.71 cal kyr BP)

This interval occurs between FLLS2 and FLLS1 and is labeled Unit 1B in the CHIRP profiles (Fig. 2). The base shows some bioturbation and mixing with the underlying gray clay layer at the top of FLLS2. The sediment at the base of this interval is similar to the pre-Tsoyowata interval; a faintly mottled yellowish to olive opaline clay in the southern sub-basin and a dark mottled to laminated clay in the northern sub-basin. Core 3A shows the most heterogeneity with 5–20 cm thick variations between medium-to-dark gray

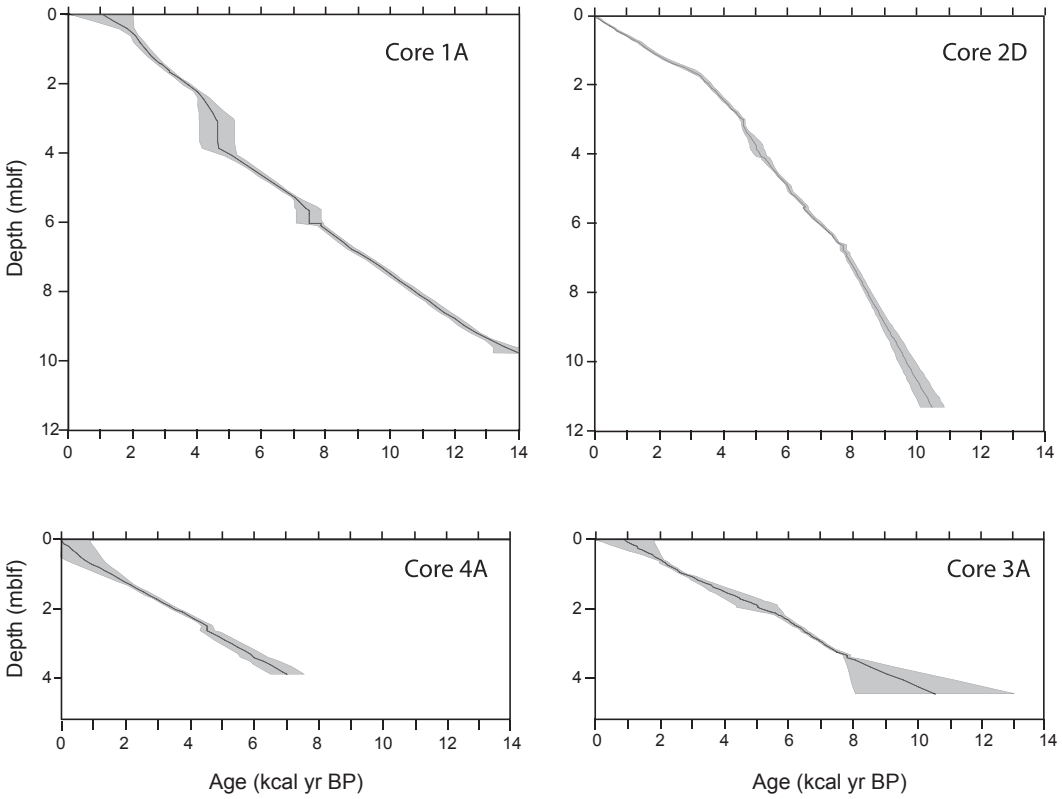

Fig. 4. Age model for 2010 piston cores. Gray envelopes show uncertainties at the 2σ confidence level.

discontinuously laminated/mottled opaline clay. As with the Pre-Tsoyawata interval, several angular pebbles of granodiorite and metavolcanics matching the lithology of the watershed and ranging from 0.5 to 3 cm diameter are found scattered within this interval. Similar occurrences of pebbles in deep lake sediments have been interpreted as the result of shore ice rafting (Zimmerman et al., 2011).

4.2.5. Most recent event turbidite FLLS1; (4.71 ± 0.14 kcal yr BP)

This turbidite is interpreted to be generated by the most recent seismic event along the West Tahoe Dollar Point Fault (Brothers et al., 2009; Maloney et al., 2013). The turbidite is thickest in core 1A (77 cm), and thinnest in core 3A (4 cm). Magnetic susceptibility peaks in the FLLS1 turbidite range from 60 × 10^{-6} SI in core 1A to 25 × 10^{-6} SI in core 2D. The age of the FLLS1 event is constrained by a composite model based on 4 cores from FLL. The preferred model has a range of 4.57–4.85 cal kyr BP (i.e. 4.71 ± 0.14 cal kyr BP), and the conservative model has a range of 2.89–5.69 cal kyr BP (Maloney et al., 2013).

4.2.6. Late Holocene post FLLS1 interval (4.71 cal kyr BP – recent)

This interval corresponds to section I, unit 1C in CHIRP data (Fig. 2) and occurs above the FLLS1. There is a sedimentologic shift in unit 1C to a lighter homogeneous olive mud from darker mottled and discontinuously laminated mud below (Fig. 5). This sedimentary shift is observed in all 4 cores but is more pronounced in the northern sub-basin, particularly in core 3A where it occurs at 134.5 cm core depth (3.64 ± 0.31 cal kyr BP). In Core 2D it occurs at a depth of 208 cm (3.65 ± 0.09 cal kyr BP). In core 2D, sediment accumulation rates are lower in unit 1C than in the older parts of the core, dropping to less than 1 mm/year, and then decreasing to 0.4 mm/year at ~3–2 cal kyr BP (Fig. 7). Magnetic susceptibility is a little higher in the lower part of this interval than it is in unit 1B (5–10 × 10^{-6} SI) and drops off to a near zero baseline (2–5 × 10^{-6} SI) above the sediment color change.

4.3. Geochemistry

4.3.1. Elemental geochemistry proxies

A number of elemental proxies were found to be useful for paleolimnological interpretations and are illustrated in Fig. 7. These include several elements (eg. Ti, K, Rb, Zr) that track together (Fig. 8) and are commonly used as detrital proxies (Kylander et al., 2011). Ca is an elemental proxy that is commonly antithetic to Fe, and has been used as a proxy for dissolved inorganic carbon in more alkaline lake systems (Kylander et al., 2011), however in FLL, the Ca tracks with the detrital proxies (Figs. 7 and 8). Fallen Leaf Lake has such low alkalinity that there is virtually no authigenic carbonate mineral phase and the Ca likely is contributed by Ca silicates transported from metasedimentary units in Glen Alpine Creek. Fe also tracks well with the clastic proxies in the turbidite layers, however Fe/Ti ratios are plotted in order to subtract the clastic component and serve as a redox proxy (Guyard et al., 2011). Plots of K, Ti, and Ca all show strong peaks associated with the turbidite intervals, silty bands, and the Tsoyowata tephra (Fig. 7). A double peak is associated with FLLS2-Tsoyowata tephra interval but only because during coring the stiff ash layer was dragged 10 cm down core. Core disturbance is limited to the 10 cm below the ash, and does not affect any other section of the core.

XRF proxies are interpreted to represent biogenic fractions in the core. The ratio of incoherent (Compton) to coherent (Raleigh) X-ray scattering intensity (inc/coh), is used as a measure of light element concentration, which can either be organic matter or pore water (Guyard et al., 2007), and Si/Ti ratios are used as a proxy for BSi (Brown et al., 2007; Brown, 2011). The inc/coh and Si/Ti proxies strongly co-vary, as seen by similar eigenvectors (blue arrows on

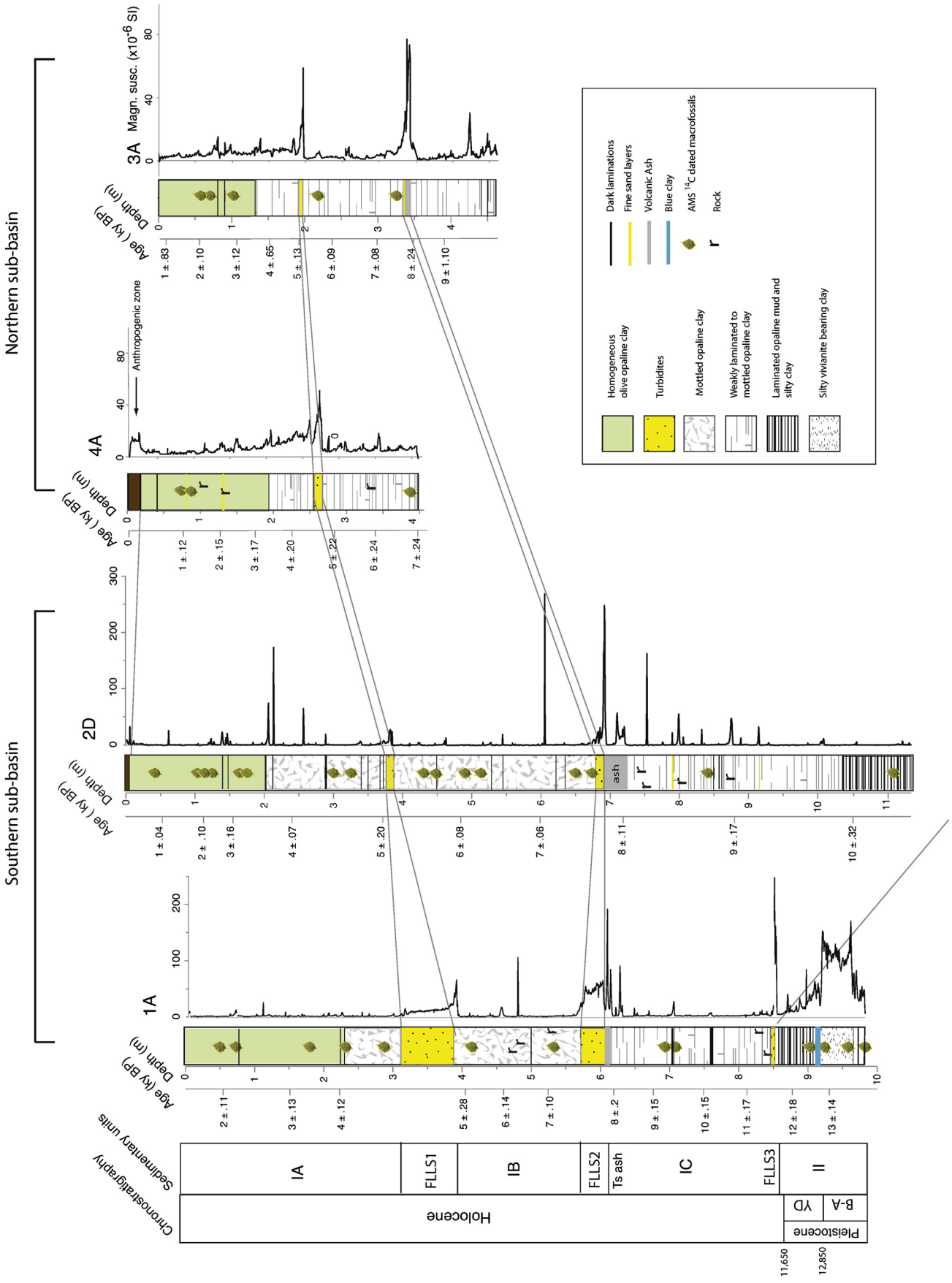

Fig. 5. Sedimentology and stratigraphic correlation of cores with magnetic susceptibility and location of ^{14}C dates.

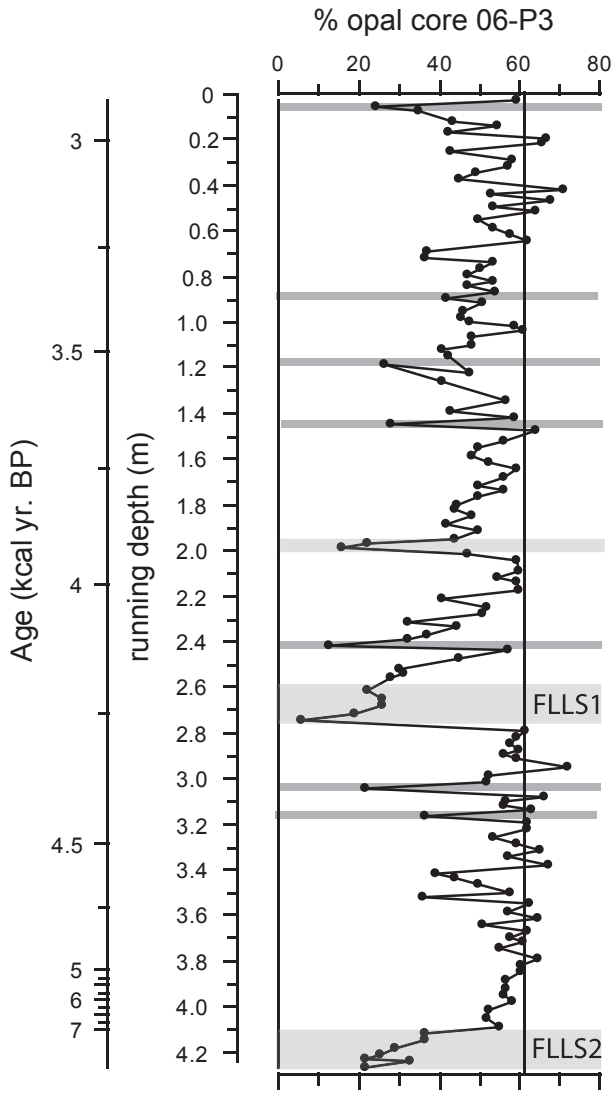

Fig. 6. Biogenic silica from core 06-P3. Shaded bands represent clastic bands and turbidites.

Fig. 8), possibly because diatoms are very porous and fluffy, compared to denser clastic material. The Si/Ti ratios from XRF data show change in relative abundance of biogenic silica down core (Fig. 7), but were not calibrated to provide values of % wt opal. However, the opal analyses conducted on core 06-P3 in the time interval from 2.91 to 7.39 cal kyr BP provide a means of determining the range of % opal (Fig. 6). The range of opal is from 6 to 35% wt. in the turbidites and thin clastic bands, and 32–72% wt. in the opaline background sediment (Fig. 6). Core 06-P3 was taken in proximity to the fault escarpment to capture the turbidites, and over-penetrated the sediment by approximately 1 m (Brothers et al., 2009). Scant age control on this core precludes precise correlation to core 2D.

4.3.2. Organic geochemistry

The interpretation of the $\delta^{13}C$ of sedimentary organic matter in freshwater lake sediments can be complex but informative if the effects of changing organic matter source material, reservoir composition, and diagenetic effects can be deconvolved. Overall trends are illustrated in a composite time–series graph produced from core 1A, 2D, and 3A data (Fig. 9). This composite graph spans the Holocene and the last ~1800 years of the Pleistocene and provides a direct inter-comparison of the isotope records between cores. Cross-plots of organic geochemical proxies (Fig. 10) allow for an additional means of interpreting organic source material. The major organic geochemical features discussed below are 1) geochemical distinctions associated with the turbidite events, 2) long-term trends in the background (non-turbidite) sedimentation that reveal geochemical evolution of this system over the past ~13 thousand years, and 3) distinct isotopically-defined zones, along with short-term trends that correspond to changes the gross stratigraphy and elemental geochemistry.

Turbidites strongly punctuate the FLL organic geochemistry record and reveal a distinct signature reflective of source material and particle sorting during deposition (Figs. 10 and 11). The composite graph (Fig. 9) shows clear TOC (%), TN (%), $\delta^{13}C$, and C:N excursions associated with FLLS1 and FLLS2, although the $\delta^{15}N$ record is insensitive to the turbidite intervals. A more detailed look at trends through the FLLS1 turbidite (Fig. 11) indicates that the coarser grained material at the base of the turbidite is ^{13}C-enriched compared to the more ^{13}C-depleted finer grained material overlying it. The white/gray clay capping the turbidite is the most ^{13}C-depleted portion of the turbidite sequence. In the FLLS2 turbidite overlying the Tsoyowata ash, the difference between the ^{13}C-enriched basal turbidite and the ^{13}C-depleted clay cap is similar (2.0‰) to that observed for FLLS1. This observation is compatible with a trend in the opal record through FLLS1 from core FLL06-P3 (Fig. 6), in that the basal sand in FLLS1 is depleted in biogenic silica, whereas the clay layer at the top of FLLS1 contains 28%. Similar % opal values were also observed in Lake Tahoe for the bases and tops of turbidites (Smith et al., 2013). If one concludes that sorting of algal and terrestrial organic matter is achieved by turbidite grading, then this indicates that algal organic matter is ^{13}C-depleted by at least 1.6‰ compared to terrestrial organic matter, and likely by a greater amount since sorting of algal and terrestrial OM by grain size is likely to be incomplete.

The composite graph (Fig. 9) reveals substantial long-term trends in the composition and amount of carbon and nitrogen accumulation that occurred in this watershed over the past ~13.9 thousand years. Both TOC (%) and C:N show gradual long-term increases through the Holocene, starting at values of 1.5 and 8.3%, respectively, in the Pleistocene and increasing to values as high as 6.4 and 11.8%, respectively, at the top of core 2D (Fig. 9). A correlation between TOC and C:N across all cores (Fig. 10C) indicates that TOC increases can be mostly explained by addition of terrigenous organic matter, which has higher C:N values compared to algal organic matter. Sedimentary inorganic nitrogen concentrations, inferred from *y*-axis intercepts (Fig. 10A), are highest for core 3A and lowest for core 1A and appear to be highest for cores with the highest sedimentation rates and TOC. This suggests that the inorganic nitrogen is most likely terrigenous. TN also consistently increases through the Holocene while ranging from approximately 0.2 to 0.5%. $\delta^{15}N$ tends towards less enriched values through the Holocene. Over this period, excluding turbidite intervals, $\delta^{13}C$ varies in magnitude by 3.6‰ (−28.5 to −24.9‰) and $\delta^{15}N$ varies by 1.8‰ (0.3–2.1‰). Of these trends, TOC, TN, and C:N steadily increase through the Holocene with minimal interruption. This same trend was also recently observed in Lake Tahoe (Smith et al., 2013). While post-burial organic matter degradation may well occur, this process alone seems unlikely to account for this trend. TOC:TN are highly correlated within (Fig. 10A) and across all cores ($R^2 = 0.87$; Fig. 10E) indicating that no significant preferential degradation of carbon or nitrogen has occurred through time. Additionally, if organic matter degradation alone accounted for the trends in TOC, TN, and C:N throughout the Holocene, a more consistent and systematic attenuation of these parameters with depth might well be expected. As such, these trends most likely reflect variations in the

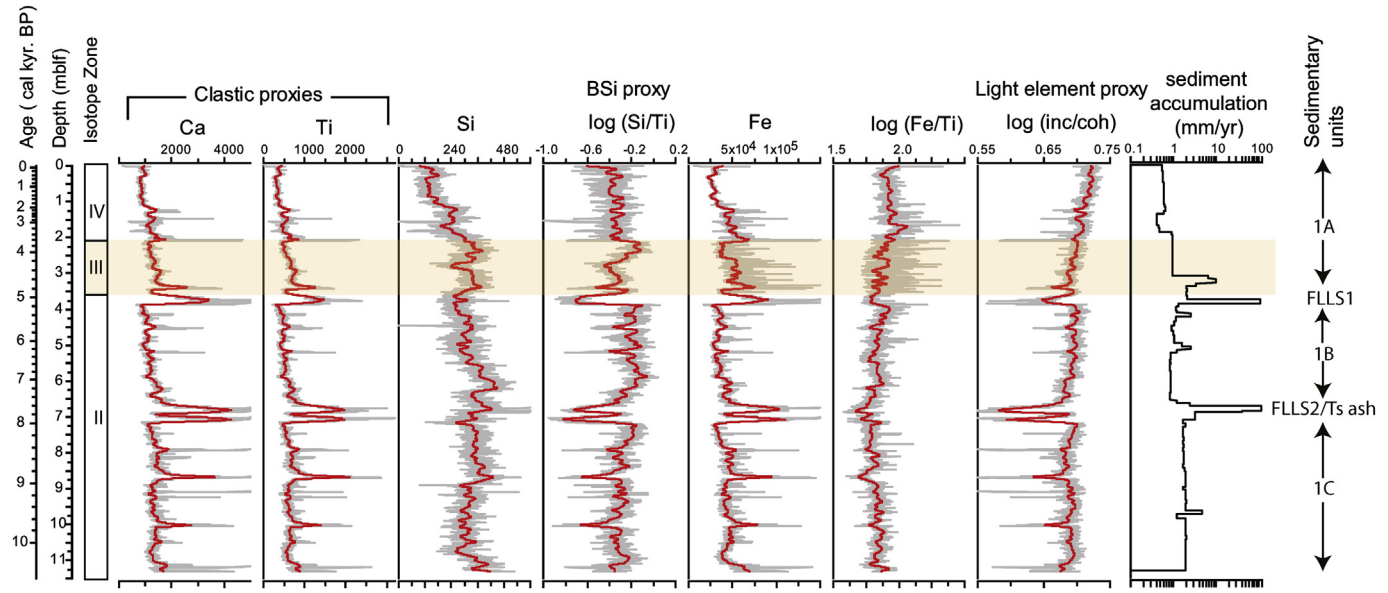

Fig. 7. Scanning XRF intensity data for core 2D of both single elements, reported in counts, and normalized log ratios of counts. inc/coh = ratio of incoherent (Compton) to coherent (Raleigh) X-ray scattering intensity. Sediment accumulation rates were calculated from the age model for core 2D. Sedimentary units and isotope zones are discussed in Sections 4.2 and 4.3.2, respectively. Lowess smoothing is shown in red. (For interpretation of the references to colour in this figure legend, the reader is referred to the web version of this article.)

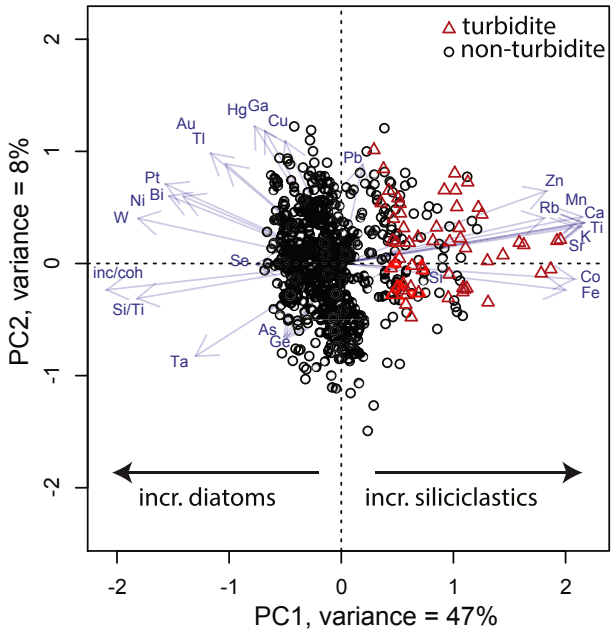

Fig. 8. Principal component analysis biplot of Scanning XRF elemental data from. a section of core 2D containing FLLS1 and background opaline clay (from 277-413 cmblf), showing elemental separation between turbidite and non-turbidite intervals. Note that the Ca eigenvector plots with typical clastic proxy elements Ti, Rb, K, and Sr on the right.

composition and amount of organic source material being delivered to the sediments. In this interpretation, the sedimentary organic geochemistry is controlled by the relative fluxes of a ^{13}C-depleted, lower C:N, higher $\delta^{15}N$ algal end-member and a more ^{13}C-enriched, higher C:N, lower $\delta^{15}N$ terrestrial end-member. This end-member delineation is consistent with the correlation of high $\delta^{15}N$ values with low C:N, and depleted $\delta^{13}C$, values (Fig. 10B, D) in our data. Goldberg et al. (2015) investigated the chemical drivers of seasonal changes in dissolved organic matter chemistry in Fallen Leaf Lake and Lake Tahoe and similarly resolved terrestrial and aquatic seasonal end-members.

The $\delta^{13}C$ record in FLL can be divided into four isotopic zones, labeled I–IV in Fig. 9, and are accompanied by shifts in $\delta^{15}N$, C:N, TOC, and TN. In Section I, from 13.5 to 11.48 cal kyr BP, $\delta^{13}C$ values decrease. In Section II, from 11.48 to 4.71 cal kyr BP, $\delta^{13}C$ remains stable, but undergoes a very gradual ~1‰ upward increase. In Section III, from 4.71 to 3.65 cal kyr BP, a sharp upward decrease in $\delta^{13}C$ occurs following FLLS1. Three of these zones can be interpreted in the context of climatic changes. The first is the trend in zone I, which is best interpreted as a change in organic matter source material during deglaciation. TOC, TN, and C:N increase rapidly while $\delta^{15}N$ tends towards more enriched values (Fig. 9). Meanwhile, the $\delta^{13}C$ curve is sinuous, moving between more depleted to more enriched values during the Younger Dryas period, before stabilizing at more depleted values (<−27.0‰) in the early Holocene.

The second zone of climatic interest is zone III, which pertains to the late Holocene neopluvial, and the subsequent change to zone IV (Fig. 9). Zone III has a pronounced depleted signature in $\delta^{13}C$, followed by an enrichment by ~2‰ at the top of isotope zone III, at 3.65 cal kyr BP. Organic matter content is lower than the interval below FLLS1, indicated by the negative baseline shift in both TOC and TN at the base of zone III (Fig. 7). Clastic proxies, including Ca and Ti in the southern sub-basin (Fig. 6), and magnetic susceptibility in the northern sub-basin (Fig. 5) show a slight increase in this zone. C:N values become slightly lower (Fig. 7), and may reflect modest changes in organic matter source. Sedimentologically, this interval is dark and mottled in texture, with the shallower cores in the northern sub-basin showing a more pronounced mottled texture. The dark color faded soon after cores were opened, and is likely the result of unstable Fe minerals, which is supported in the high level of variance in the normalized Fe signal (Fig. 6).

Several processes could plausibly explain the more negative (depleted) $\delta^{13}C$ excursion in Zone III: (1) lower sedimentary fluxes of terrestrial vs. algal organic matter (2) enhanced lake mixing, or

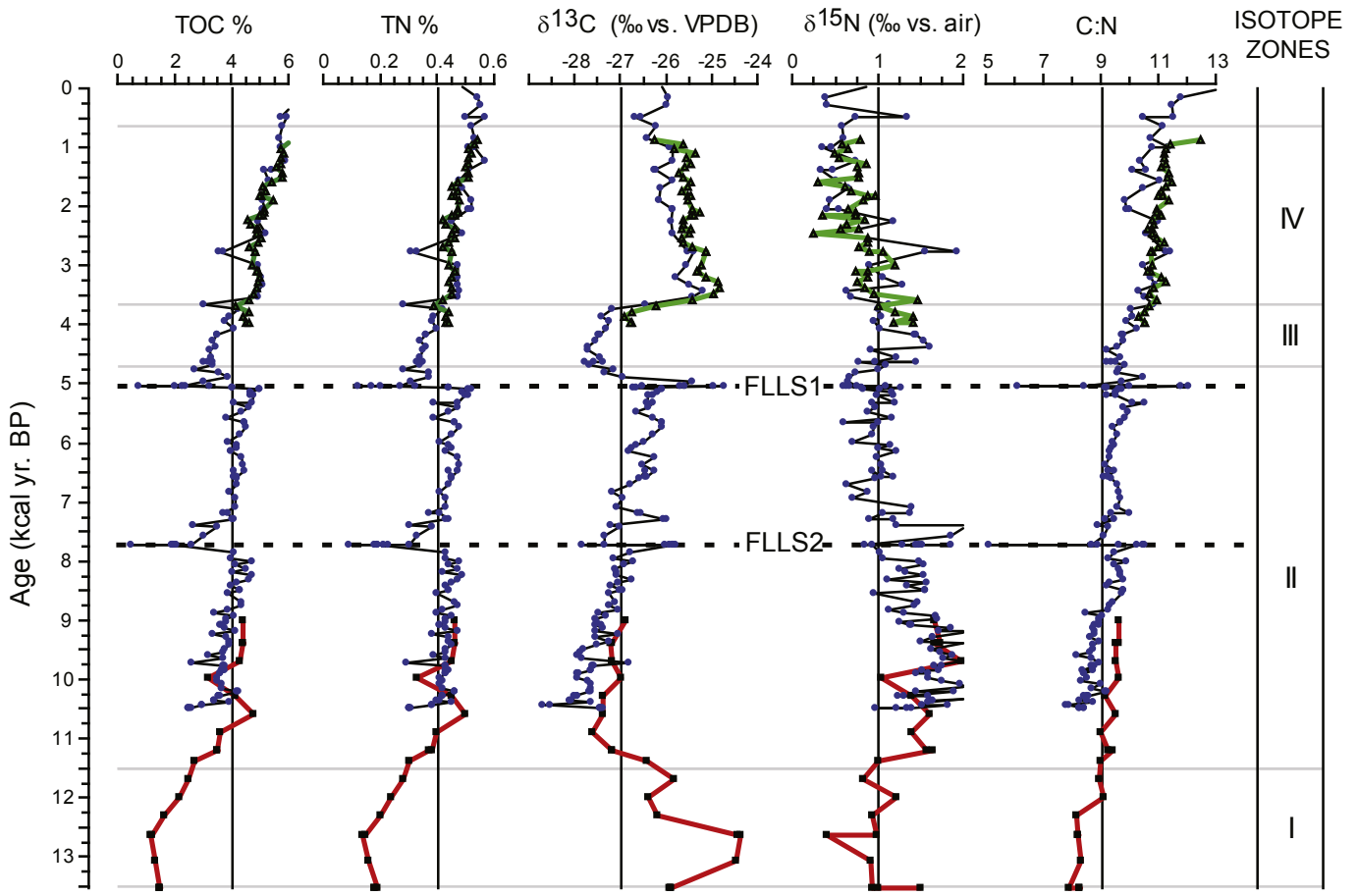

Fig. 9. Composite plot of organic geochemistry from cores 1A (red), 2D (blue), and 3A (green). (For interpretation of the references to colour in this figure legend, the reader is referred to the web version of this article.)

(3) decreased CO_2 utilization rates. Reduced terrigenous vs. algal input would lead to more depleted ^{13}C values because in this system terrestrial OM is ^{13}C-enriched compared to algal OM. Supporting this interpretation, C:N values are also lower in Zone III. Increased mixing could also lead to this negative excursion by increasing transport of ^{13}C-depleted CO_2, originally derived from the respiration of ^{13}C-depleted organic matter, to the epilimnion. Depleted $\delta^{13}C$ values could also result from increased CO_2 concentrations, or lower primary productivity, which would lead to lower utilization of the epilimnion CO_2 reservoir and a more complete expression of the ~−20‰ fractionation associated with biosynthetic carbon fixation (Cohen, 2003). In this freshwater system, algae can fix either (1) dissolved CO_2 in equilibrium with the atmosphere ($\delta^{13}C_{air} \approx -8‰$) or (2) CO_2 that is derived from the aqueous respiration of isotopically light terrestrial carbon. This is in contrast to marine systems where bicarbonate is the principal carbon source for aquatic algae (Meyers, 1994). Lastly, the expression of kinetic isotopic effects can be suppressed as the supply of dissolved CO_2 is exhausted, such as during blooms when rapid uptake of CO_2 occurs. In light of these processes, the negative $\delta^{13}C$ excursion in Zone III most likely reflects a period of (1) higher algal and lower clastic flux into the lake and, possibly, (2) more frequent and complete lake mixing. Since CO_2 concentrations and absolute rates of algal productivity are not known, it is difficult to assess whether CO_2 utilization was significantly different in the past. More frequent and complete mixing should increase nutrient and CO_2 fluxes to the epilimnion and lead to a generally larger epilimnion CO_2 reservoir. This would generally favor lower utilization rates and disfavor expression of reservoir effects, which would otherwise shift the $\delta^{13}C$ of algal OM towards more positive values that could ultimately approach those of CO_2 ($\approx -8‰$) if 100% utilization was achieved. Indeed, the sedimentary $\delta^{13}C$ record does not evidence utilization rates of this magnitude and this suggests that CO_2 limitation is not a key driver of sedimentary OM $\delta^{13}C$ in this particular system.

Zone IV is characterized by shifts in %TOC and TN, and C:N, where 3.65 cal kyr BP marks the start of positively increasing trends in these three proxies (Fig. 9). The positive trend in C:N appears to reflect increasing terrestrial vs. algally-derived organic matter contributions to the sediments, which would reflect decreased amounts of algal productivity relative to terrestrially-derived inputs. The elemental geochemistry corroborates this interpretation with several proxies, including Fe, Ti, and Ca (Fig 6), indicating an increase in clastic input.

4.4. Holocene sedimentary architecture

A detailed look at the CHIRP data provides insights into the development of the Holocene sedimentary package, including the timing and growth of a sedimentary bulge in the southern subbasin, and changes in sedimentation rates over time. The Early Holocene 11.48–7.93 cal kyr BP pre-Tsoyowata interval (unit 1C in Fig. 2) shows that a sedimentary bulge began forming on top of the fairly flat upper surface of the Pleistocene glaciolacustrine package (Fig. 2). Reflectors within unit 1C converge as they move away from the basin center, towards the perimeter and unit 1C is considerably

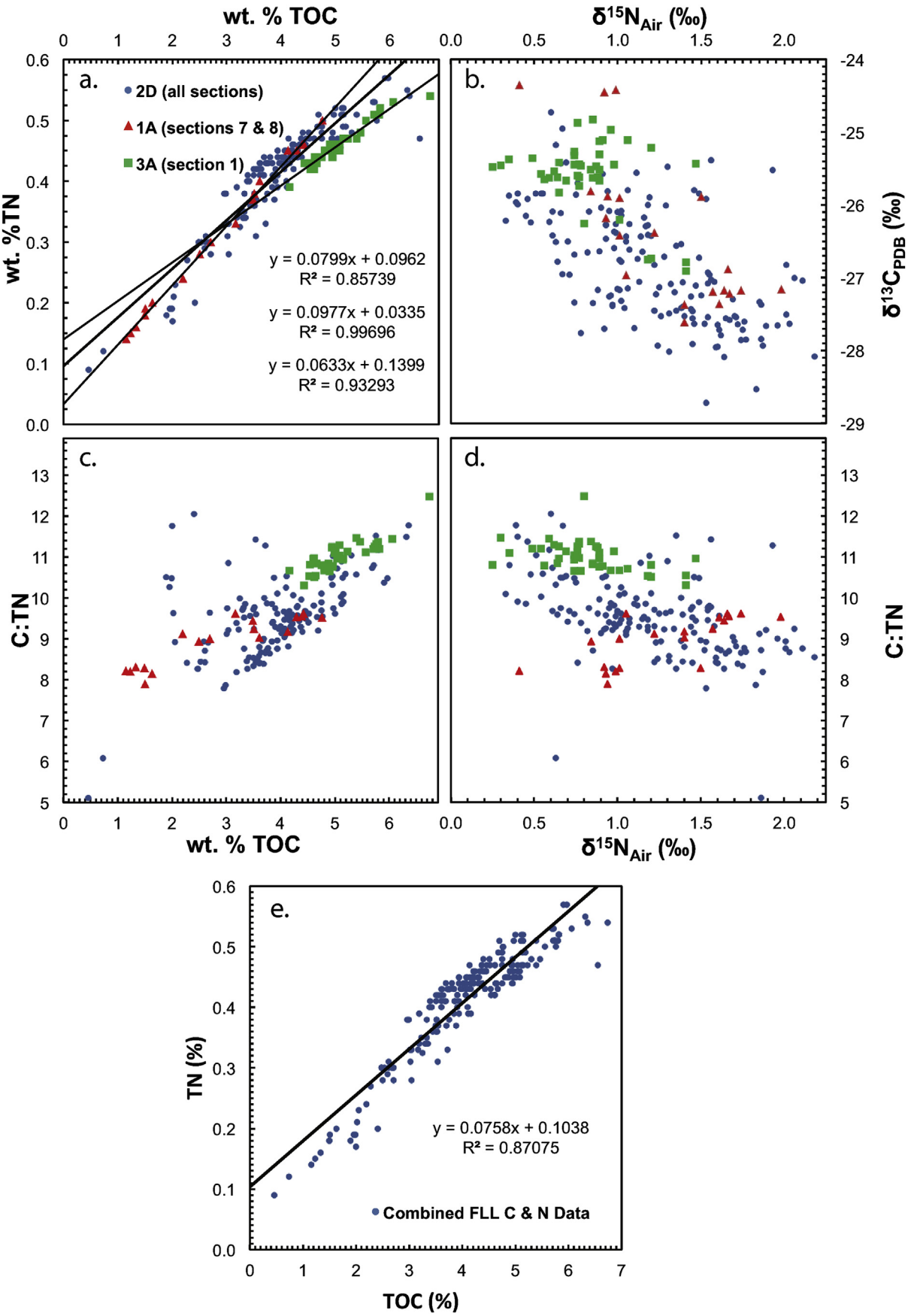

Fig. 10. Cross-plots of bulk measured organic geochemical parameters, broken down by core in plots a-d and for all samples in plot e. The intercepts of the linear regressions shown in plot a indicate the amount of nitrogen assumed to be present in the absence of carbon and provide an estimate of average total inorganic nitrogen (TIN) present in samples analyzed from each core.

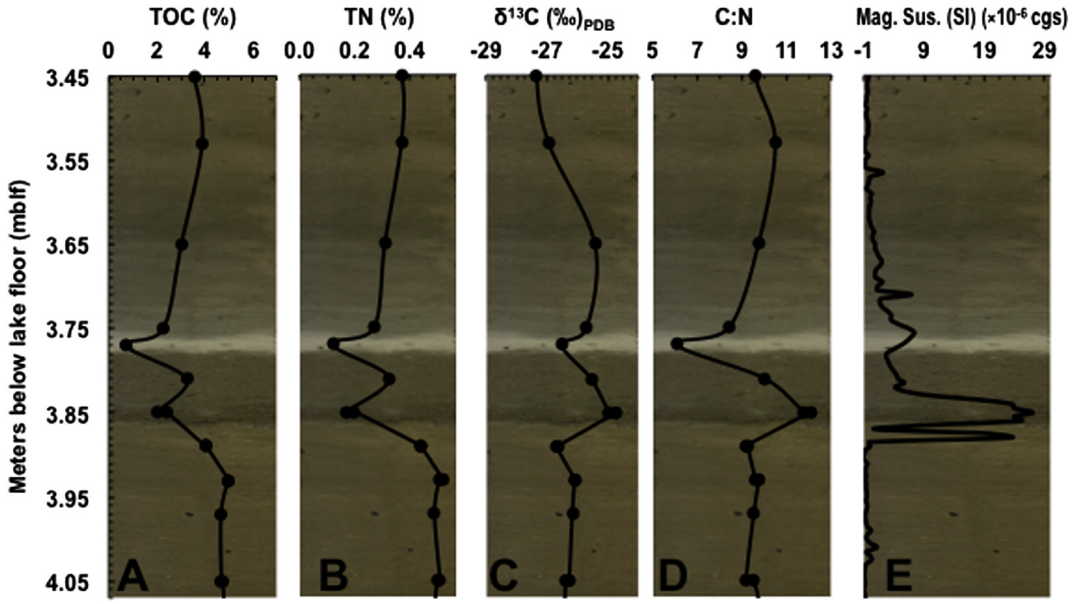

Fig. 11. Elemental and isotopic analyses and magnetic susceptibility across FLLS1 (3.75–3.86 mblf) as preserved in core 2D, plotted by depth. The plots are each underlain by the same photograph of the core segment. The turbidite has a dark, sandy base and an organic rich top overlain by a gray clay. $\delta^{15}N$ values did not appear to be significantly affected across the turbidite.

thinner in core 1A in the moat along the perimeter of the basin floor. The calculated mean sediment accumulation rate for the early Holocene, unit 1C, in the center of the basin (in core 2D) is 1.9 mm/year, whereas the average rate in the moat (core 1A) is only ~0.6 mm/year. Background (i.e. non-turbidite) sedimentation rates in the moat do not change appreciably throughout the remainder of the Holocene, but in 2D they decrease. The sedimentary bulge continued to grow more slowly during the mid Holocene, during the post-Tsoyowata interval (unit 1B) from 7.75 to 4.71 cal kyr BP, with the average sediment accumulation rate dropping to about half (1 mm/year) in core 2D. The CHIRP reflectors within unit 1B converge slightly towards the basin floor perimeter, although not as strongly as in unit 1C. FLLS1, deposited on top of unit 1B has a leveling effect on the basin floor through partially filling in the moat, as seen by the wedge shape of FLLS1 (See Fig. 7 in Maloney et al., 2013). Whether the result of basin leveling, or a change in basin circulation, unit 1A has a more blanketing geometry, where internal reflectors show little convergence from the basin center towards the basin floor perimeter. Unit 1A also has the lowest mean sediment accumulation rate (Fig. 7), particularly in the basin center where it drops to about half of the rate of unit 1B (~0.5 mm/year).

In the northern sub-basin, although the Holocene package is thinner, subtle changes in sediment aggradation and accumulation rate can be discerned. Particularly, the northern sub-basin contains multiple morainal ridges that transect the lake to create intra-morainal pockets. During the Pleistocene these ridges were areas of high relief and they show no sign of sediment preserved on their tops. The southernmost intra-morainal pockets were cored (sites 3A, 4A) and provide age constraints of the thickness of the Holocene package. Unit 1C largely bypasses the tops of the morainal ridges and fills in pockets in-between the ridges (Fig. 2). In the two cored intra-morainal pockets (locations of cores 3A and 4A in Fig. 2) the calculated sediment accumulation rate is greater in unit 1C than in 1B. Unit 1B aggrades above the top of one of these ridges (morainal ridge directly north of core 4A, Fig. 2) and also shows onlap onto a ridge the northernmost pocket cored (ridge north of core 3A, Fig. 2), In contrast, unit 1A shows a more blanketing geometry, and uniform thickness in the flatter centers of these pockets.

Four detailed reflectors (A1-A4 inset to Fig. 2) that are traceable throughout the southern sub-basin can be identified in core 2D and are discussed in relation to the geochemical data. The base and top of zone III correlate with seismic reflectors A4 and A2 respectively. Seismic reflectors A4 and A2 also correspond to both sharp drops in BSi and spikes in clastic proxies (Fig 12) and may be highlighting depositional events at the base and top of the zone. Within zone III there is a general increasing trend in Si/Ti, the proxy for BSi. The lower two thirds of zone III show lower Si/Ti than below Zone III and the upper third of zone III shows an increase in Si/Ti (Fig 12). Interestingly, reflector A3 occurs in the middle of zone III, and marks where Si/Ti begins to increase. A3 may represent a change in density difference indicated by a higher % of BSi (and higher diatom productivity) in the uppermost half meter of zone III. The age model for core 06-P3 is not sufficient to provide detailed correlation to specific horizons in core 2D, however, zone III is roughly equivalent to a running depth of 2.6 to ~1.5 m in core 06-P3, and the opal silica pattern in core 06-P3 does support the pattern of lower BSi in the base, and higher in the top, of zone III, (Fig. 6). Si/Ti drops to a lower baseline in Zone IV marking a transition to lower rates of diatom productivity vs. clastic runoff in zone IV, which is interrupted by a brief spike at the start of the little ice age, at 42 cm (Fig. 12).

5. Late Pleistocene–Holocene climate signals

5.1. Late glacial-Holocene transition

The end of Late Tioga glaciolacustrine sedimentation in the Tahoe basin appears to be synchronous with deglaciation further to the south in the Sierra Nevada. The top of the silty blueish vivianite-bearing sediments in core 1A is 12.43 ± 1.7 cal kya BP, and these glaciolacustrine sediments transition into laminated silty clay of Younger Dryas age. The top of the glaciolacustrine-Younger Dryas interval in FLL, punctuated by FLLS3 (11.48 ± 1.7 cal kyr BP), is correlative with Event O of Smith et al. (2013) (11,845 ± 645 cal kyr BP) in Lake Tahoe that likewise bounds the glacial-postglacial packages. The last significant Pleistocene glacial advance in the Sierra Nevada is referred to as the Recess Peak advance, recorded by

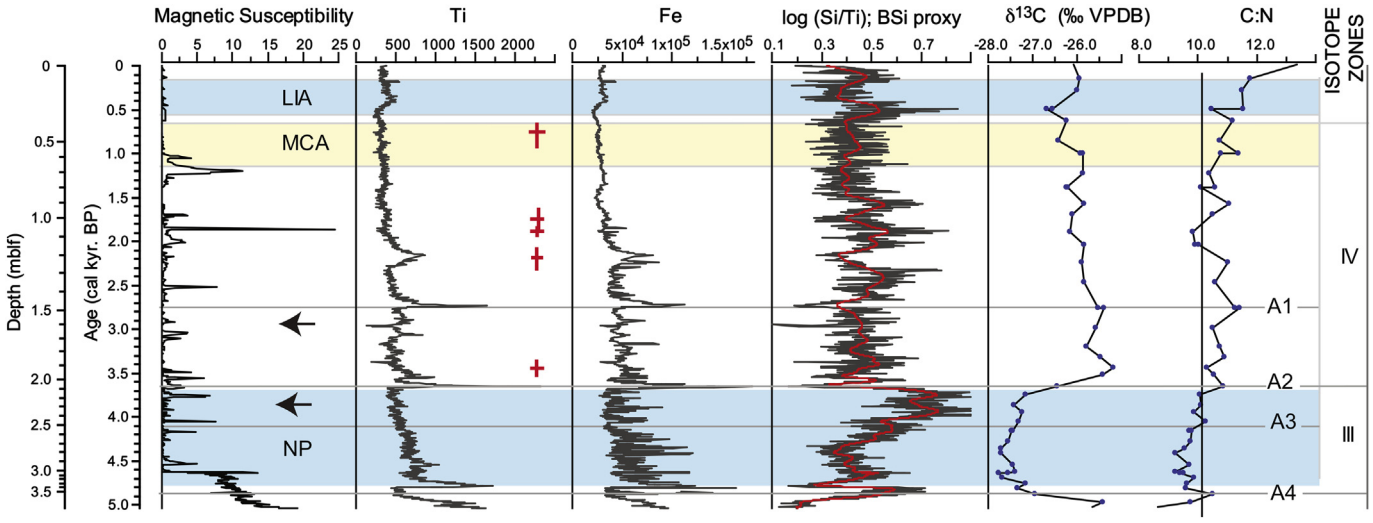

Fig. 12. Summary figure of selected proxies and regional climate data above FLLS1 (Last 5 ka) for core 2D. Crosses to the right of the Ti curve indicate drowning ages of submerged trees in FLL (from Kleppe et al., 2011) where vertical length is minimum and maximum, and horizontal line is the mean. Tree cluster associated with the end of the Medieval climate anomaly is represented by topmost cross. Arrows are median ages for the highstand dates from Briggs et al. (2005) at Pyramid Lake. NP = neopluvial, LIA = Little Ice Age, MCA = Medieval Climate Anomaly. A1 – A4 are seismic reflectors shown in Fig. 2, and A4 occurs above FLLS1.

moraines throughout the Sierra Nevada. Ages on basal lake sediments above the terminal moraine indicate that the advance began by ~14.2 cal kyr BP and ended before ~13.1 cal kyr BP (Clark and Gillespie, 1997). Cosmogenic ^{36}Cl dates of exposure surfaces of Recess Peak terminal moraines in Bishop Creek in the southern Sierra Nevada range from 12.5 ± 0.7 to 13.1 ± 1.2 cal kyr BP (Phillips et al., 2009) and overlap with the age of retreat indicated by Clark's paleolimnological work.

5.2. Early and mid Holocene 11.6–5 cal kyr BP

Following the Younger Dryas, a cold interval in the Great Basin and Sierra Nevada, the Early Holocene is characterized as a cool and moist time, with abundant pluvial lakes in the Great Basin (Grayson, 2011). Chironomid-based summertime temperatures from the central Sierra Nevada show a postglacial warming trend from 14.8 to 10 cal kyr BP, which is interrupted by a 500 year interval (~12–11.5 cal kyr BP) where lake temperatures were depressed by ~0.5 °C, and interpreted to be a localized expression of the Younger Dryas stadial (Porinchu and MacDonald, 2003). Wet conditions persisted in the western Great Basin through at least 7.5 cal kyr BP, if not ~6.5 cal kyr BP giving way to the mid Holocene dry period (Grayson, 2011), with an uptick in fire history between 7.5 and 7 cal kyr BP in the Tahoe basin (Beaty and Taylor, 2009). The FLL record, from a gross sedimentologic standpoint is fairly indistinct through these periods, yet a few general observations can be made. The sedimentation rate in core 2D is highest in the early Holocene. During this interval, a sedimentary bulge was developed in the depocenter of the southern sub-basin, as indicated by the high sedimentation rates of ~2 mm/year in core 2D, relative to core 1A in the moat. Laminations were developed and preserved in the early Holocene, a function of preservation and lack of bioturbation, which may indicate ice cover and resulting winter stratification. The early Holocene also shows a greater abundance of pebbles in the FLL cores. The pebbles may have entered the lake through rafting from shore ice during times when the lake may have iced over. Similarly, the presence of pebbles in mid Holocene indicates at least some cold winters during this period. Carbon and nitrogen elemental and isotopic data show gradual trends and inflections through this period that are difficult to fully interpret given available information.

5.3. Late Holocene neopluvial period

5.3.1. Review of evidence from the Great Basin; ~5–3.7 cal kyr BP

There is strong evidence of a Late Holocene wet period in the Great Basin of western North America, both from lake core and shoreline records. In the Great Basin, increases in effective moisture during the late Holocene are recorded by resurgences in marsh and grasslands, as well as by neoglacial advances and neopluvial episodes that began between 5 and 3.5 cal kyr BP (Adams et al., 2014; Grayson, 2011; Mensing et al., 2004). Submerged trees in Lake Tahoe that grew on exposed lakeshore below the elevation of the natural sill during the mid Holocene show drowning ages ranging from 4.8 to 5.7 cal kyr BP (Lindström, 1990), and the pollen record from Little Valley meadows, located in the Carson Range east of Tahoe records cooler and wetter conditions starting ~4 cal kyr BP (Wigand and Rhode, 2002). Collectively, these records indicate increases in effective moisture in the Great Basin and Sierra Nevada, although spatially heterogeneous and initially intermittent, starting at ~6 cal kyr BP, and becoming more widespread and persistent from 5 to 4 cal kyr BP.

Walker Lake in western Nevada possesses one of the older records of the transition between the drier middle Holocene and the relatively wet late Holocene in the Great Basin. The age model reported in Benson et al. (Benson et al., 1991) indicates that the basin began filling as early as ~4.7 cal kyr ^{14}C BP (~5.4 cal kyr BP), although additional dates to confirm this age model are vital. Walker lake then reached a highstand at about 3.7 cal kyr BP (Adams et al., 2014). Four subsequent highstands in Walker Lake over the last 4 ka have been documented by Adams (2007) and dated by ^{14}C of wood and plant remains in lacustrine outcrops along the lower Walker River, and at least one desiccation event between 2.5 and 2 cal kyr BP (Adams, 2007; Benson et al., 1991; Bradbury et al., 1990; Dong et al., 2014) indicates that the late Holocene also experienced prolonged drought episodes interspersed with the wet intervals. A complicating effect of interpreting climate from fluctuations in Walker Lake levels, however, is that the Walker River has repeatedly been diverted out of and back into the Walker Lake basin in the late Holocene (Adams, 2007; King, 1993). The point of diversion is located just north of the town of Yerington, NV, where a paleochannel splits off the main Walker River channel

and flows through Adrian Valley to become a tributary to the Carson River. The exact reasons for the river switching between these two channels are unknown, but it may have to do with the occurrence of floods and debris blocking one channel or the other.

Pollen records also document the transition out of the middle Holocene and into the late Holocene. Records dated to ~4.7 cal kyr BP show resurgence of the Ruby Marsh in eastern Nevada (Thompson, 1992) and grasslands in the vicinity of both Fish and Wildhorse lakes (Mehringer, 1985). Pollen records also indicate wetter conditions between 4 and 2 cal kyr BP in the Carson Sink (Wigand and Mehringer, 1985).

On the younger side is the age of a highstand in Mono Lake, eastern California at 3.77 cal kyr BP (Stine, 1990) and in Diamond Pond in east central Oregon at 3.7 cal kyr BP (Wigand, 1987). In the alpine environment, increased winter precipitation and cooler summer temperatures related to changes in seasonal insolation are reported to have triggered the onset of neoglacial advances in the central Sierra Nevada at ~3.2 ka (Bowerman and Clark, 2011).

Pyramid Lake is the Great Basin lake most relevant to the precipitation history of the Lake Tahoe watershed because it resides in a closed basin at the terminus of the Truckee River. Pyramid Lake reached an elevation of about 1182 m in the late 19th century but has since receded to an elevation of about 1157 m due to upstream water diversions and consumption (Adams, 2012). Pyramid Lake-level history serves as a proxy for winter precipitation in the subalpine environment of the Lake Tahoe basin because the majority of water flowing into Pyramid Lake comes from melting of Sierra Nevada snowpack. Three studies of significance weigh in on this subject. First, work on oxygen isotope geochemistry by Benson et al. (2002) in Pyramid Lake shows highly enriched values of $\delta^{18}O$ that are interpreted to represent a mid Holocene dry period. During this time, the level of Lake Tahoe would have dropped below its natural sill at the outflow to the Truckee River, currently ~2 m below the modern maximum lake level of 1898.65 m, cutting off one of the major sources of inflow into Pyramid Lake. Benson et al. (2002) estimated the timing of the mid Holocene dry period to range from about 6.5 to 3.8 cal kyr BP. However, other evidence including shoreline data and pollen records from Pyramid Lake cores indicates that the aridity period ended earlier than 3.8 cal kyr BP (Briggs et al., 2005; Mensing et al., 2004). Pyramid Lake pollen records indicate that the mid Holocene dry period ended sometime between 5 and 3.5 cal kyr BP, and that by 3.4 cal kyr BP there was intermittent filling of Pyramid Lake from the upper part of the watershed (Mensing et al., 2004).

Additionally, work by Briggs et al. (Briggs et al., 2005) on Pyramid Lake shoreline deposits indicates either one or two late Holocene highstands. Charcoal samples in a soil horizon directly below the transgressive surface show that the first highstand began after ~4.7 cal kyr BP, and although age constraints on the shoreline were too scant to reconstruct a lake–level curve, the lake reached an elevation of 1187 m at ~3.6 ± 0.35 ka ^{14}C BP (3.85 ± 0.15 kcal yr BP) and 1195 m at 2.64 ± 0.40 ka ^{14}C yr BP (2.78 ± 0.07 cal kyr BP). Collectively, Pyramid Lake, along with other Great Basin data support at least two late Holocene wet periods after 3.8 cal kyr BP in the Tahoe-Pyramid watershed following the mid Holocene dry period.

5.3.2. Evidence from Fallen Leaf Lake 4.71–3.65 cal kyr BP

The late Holocene neopluvial period in Fallen Leaf Lake corresponds to an interval in the lower part of unit 1A, following the FLLS1 turbidite, and corresponds to isotope zone III, a geochemically distinctive interval in both inorganic and organic proxies present in both the northern and southern sub-basins (Figs. 7, 9 and 12). In this time period proxy evidence indicate higher algal productivity vs. terrigenous runoff. There may have also been enhanced lake mixing and, possibly related, lower utilization of the epilimnion CO_2 reservoir, as discussed in Section 4.3.2. In the context of a wet period, enhanced lake mixing may have resulted from a shortened or weakened period of stratification. FLL is a monomictic system that is stratified from late spring to mid autumn (Noble et al., 2013). Cool spring temperatures and a larger winter snowpack could attenuate runoff pulses, sustaining runoff later into the year while reducing the likelihood that abrupt, landscape-scouring melt-water pulses enriched in terrestrial organic matter would enter the lake. This more sustained supply of cold melt water, in concert with colder air temperatures, could delay stratification while prolonging and enhancing winter and spring diatom productivity. Also, cooler and windier summer conditions, or early fall storms, could weaken or shorten the stratification period and enhance mixing conditions. Changes in organic matter source are likely a significant factor, and in zone III, aquatic algae may simply represent a larger fraction of sedimentary organic matter, compared to the shift to higher and increasing C:N ratios in zone IV (Fig. 9). The negative $\delta^{13}C$ values in isotope zone III are presently interpreted to be consistent with cooler conditions and lower quantities of terrestrial organic matter relative to algal-derived organic matter. Cooler conditions may have enhanced CO_2 solubility, delayed lake stratification, and promoted mixing. Terrestrial organic matter runoff into FLL may have been attenuated by (1) the presence of less terrestrial material in the watershed, possibly due to more persistent snow cover, or by (2) less effective mobilization of terrestrial organic matter into the watershed, possibly caused by attenuated annual snowmelts.

5.4. Late Holocene positive PDO phase 3.65 cal kyr BP – present

From a regional standpoint, a major shift in climate regime is reported to have taken place between the mid to late Holocene, although the spatial and temporal variations are complex (Barron and Anderson, 2011; Barron et al., 2012). Decreasing summer insolation in the mid to late Holocene (Berger and Loutre, 1991) was a major control that could have far reaching climatic effects in western North America during this period, including changes in winter precipitation in the Northern Sierra Nevada. In addition, Barron and Anderson (2011) attribute these changes to a shift in the strength and location of the Aleutian low during the winter, circa 4 cal kyr BP, resulting in changes in the pattern and strength of El Nino Southern Oscillation (ENSO) patterns over time. The mid Holocene, particularly the latter part from 6.3 to 4.5 cal kyr BP, represented a pattern that would have manifested itself as drier winter conditions in the southwestern United States corresponding to mid Holocene aridity in the Sierra Nevada and Great Basin. In their scenario, the late Holocene represents a pattern with more variable winter precipitation and El Nino-like conditions, such as the cooler, wetter conditions indicated by the regional proxy records they summarize.

Based on our age model, a major climate shift from mid to late Holocene occurs at 3.65 cal kyr BP in the Tahoe Basin, and is the largest change in the FLL Holocene record. It corresponds to both a sedimentologic and geochemical shift as sediments change from mottled darker opaline clay to a homogeneous olive clay (Fig. 5) with lower BSi content (drop in Si:Ti), and sediment accumulation rates drop discernibly by over 50% from >1 mm/year during the early and mid Holocene to ~0.5 mm/year throughout the Late Holocene (Fig. 6). The sediment composition after 3.65 cal kyr BP, in the lower part of Zone IV, shows an increase in clastic components and a decrease in the BSi (Fig 7). Decreased terrestrial vs. algally-derived organic contributions to the sediments in Zone IV (Fig. 9) also support suppressed algal productivity. In contrast to the late Holocene neopluvial period (Zone III) the interval after 3.65 cal kyr BP (Zone IV) may

represent the subalpine response to predominantly drier winter conditions.

Superimposed on these observed late Holocene millennial-scale trends are several sub-millennial features that capture known climatic events. Mensing et al. (2004, 2013) note variability in the late Holocene, starting at 3.4 ka, between prolonged centennial scale droughts and intense wet periods. One such interval spanning ~2800-1850 cal yr BP is termed the Late Holocene Dry Period, and is presently recognized in seven localities in the Great Basin. The Late Holocene Dry Period is recorded by the desiccation of meadows and lowering of lake levels. The effect of the Late Holocene Dry Period appears to have been more intense in the western Great Basin versus the eastern part (Mensing et al., 2008) where FLL is located.

Fallen Leaf Lake also provides evidence of variability between wet and dry periods after 3.65 ka. In Fallen Leaf Lake there are over 80 submerged trees that are attributed to lowered lake level during periods of prolonged drought (Kleppe et al., 2011), in two periods, centered around 1.8 cal kyr BP and 0.75 cal kyr BP (Fig. 12). Two older trees with drowning ages of 2.32–2.06 and 3.56–3.38 cal kyr BP indicate older drought events (Kleppe et al., 2011). In this scenario, during prolonged droughts associated with the Late Holocene Dry Period, and the Medieval Climate Anomaly (MCA; 0.650–1.150 cal kyr BP), Fallen Leaf Lake would drop ~40 m to a level at or near the top of Lake Tahoe and then return to its current level at ~1940 m after the drought ended. All of these tree clusters post-date the late Holocene neopluvial Period (Fig. 12), and support prolonged drier periods interspersed with either wet periods or short-lived high precipitation events capable raising lake level and drowning trees.

Despite the large fluctuations in lake level indicated by the drowned trees, the effects of drought on lake productivity and sedimentology, and thus on sediment core proxies in a subalpine lake environment are not as pronounced as those in the terminal lakes. The FLL cores provide only a subtle signal associated with the Late Holocene Dry Period and MCA, although higher resolution analyses may eventually reveal additional signals. The lowest sediment accumulation rates in core 2D occur in the late Holocene, dropping below 1 mm/year, and the lowest rates in core 2D may be coincident with the Late Holocene Dry Period, between ~2.8 and 2 cal kyr BP, where they drop even lower to ~0.4 mm/year (Fig. 7). Geochemically, there are some inflections in the BSi (Figs. 6 and 12), however these cannot be precisely correlated to tree clusters. The sedimentary interval corresponding to both the Late Holocene Dry Period and the MCA does not appear appreciably different above or below these periods although there are some subtle geochemical inflections in clastic proxies, especially at the base of the Late Holocene Dry Period (Magnetic Susceptibility, Ca, Ti, Fe; Fig. 12). One possible reason for the lack of drought evidence in the cores is that the geochemical proxies studied may be insensitive to picking up drought signals in this lake system. In general, it can be expected that despite the evidence for prolonged lowstands in excess of 200 years (Kleppe et al., 2011), the effects of drought in a subalpine lake environment would not be as pronounced as those in the terminal lakes in the Great Basin. Despite the large fluctuations in lake level, as indicated by the groupings of drowning ages in the trees, the effects on lake productivity and sedimentology may have been small between drought and nondrought states. An alternative scenario is to view the lowstand state in FLL as the norm, and not the anomaly during the 3.65-0.55 cal kyr BP interval. The whole of the late Holocene until 0.55 cal kyr BP may actually represent an interval that was predominantly dry, with lake levels close to the level of Lake Tahoe, interrupted periodically by sufficiently high precipitation times that resulted in intermittently recurrent short-lived lake level rises capable of drowning trees.

6. Conclusions

Fallen Leaf Lake preserves a sedimentary record of the transition from the last glacial period into the Holocene and a relatively thick Holocene sequence in the subalpine environment of the Lake Tahoe basin. The abundance of trees in this mountainous watershed has afforded high quality age models for four cores in the lake. Sedimentation rates are highest in the southern sub-basin, and the best age model is associated with core 2D, on which we have performed both organic and inorganic geochemical analyses in an attempt to capture the major Holocene climate signals. Situated at the upstream end of the Tahoe-Pyramid Lake watershed, this lake provides a great opportunity to corroborate and clarify the timing and nature of climate signals reported previously from Pyramid Lake and the western Great Basin. The two largest signals in the core are the transition from the Late Tioga glaciation, at 11.48 cal kyr BP, and the end of the late Holocene neopluvial Period at 3.65 cal kyr BP. A geochemically distinctive interval, isotope zone III, with strongly depleted $\delta^{13}C$ and lower C:N values coincides with the late Holocene neopluvial Period from 4.71 to 3.65 cal kyr BP, and is interpreted to represent a period of higher winter precipitation and relatively elevated algal productivity corresponding to a highstand previously observed in shoreline data from Pyramid Lake and other regional records.

Following the late Holocene neopluvial period, the Lake Tahoe basin enters into a different climatic state with variable precipitation that lasted for ~3 ka. During this time there is evidence that FLL lake levels lowered at multiple times, to near the level of Lake Tahoe. The homogeneous nature of sediment during this interval, coupled with low sedimentation rates and steadily increasing contributions of terrestrial organic matter suggest that the lowstand state of the Fallen Leaf Lake may have been the norm, punctuated by short term high precipitation years or multi-year intervals capable of raising lake level sufficiently to drown trees. This 3 ka interval encompasses the Late Holocene Dry Period of Mensing et al. (2013) and the Medieval Climate Anomaly. The top of this climatically variable interval is marked by the onset of the Little Ice Age, which like the neopluvial period, is signified by an increase in BSi and depleted $\delta^{13}C$ and lowered C:N values.

Contributions by authors

Specific contributions are as follows; Project leader-Noble, Design of 2010 coring campaign - Noble, Karlin, Kent; Initial core descriptions and core processing – Noble; Magnetic susceptibility data analysis Karlin, Noble; XRF data analysis – Noble; organic geochemistry analyses – Ball; ^{14}C preparation and analysis - Noble, Zimmerman; Oxcal age model and opal silica analysis- Smith; CHIRP data acquisition and processing: Maloney, Driscoll, Kent, Karlin. All authors contributed to the interpretations and writing the manuscript.

Acknowledgments

We thank Anders Noren and Kristina Brady (LRC, Univ. MN) who deployed the Kullenberg coring system at FLL, directed our coring operations, and provided lab training and support at the LRC. Thanks also to LRC staff members A. Myrbo, R. O'Grady, and J. Heck who provided helpful advice during core processing. Thanks to M. Rosen for logistical support and advice during our planning stages, to L. Stratton for coordinating coring operations and help with initial core processing, to J. Kleppe for additional logistical advice and lake access. This project was funded by National Science Foundation grants EAR-127499 and OCE-0649410, U.S. Geological Survey National Earthquake Hazards Reduction Program grants

10HQPA1000, 06HQGR0064, and 02HQGR0072, Lawrence Livermore National Laboratory, Directed Research and Development grant 09-ERI-003, Department of Defense (DoD) National Defense Science and Engineering Graduate (NDSEG) Fellowship 32 CFR 168a, and the Edna Bailey Sussman Foundation.

References

Adams, K.D., 2007. Late Holocene sedimentary environments and lake-level fluctuations at Walker Lake, Nevada, USA. Geol. Soc. Am. Bull. 119, 126–139.
Adams, K.D., 2012. Response of the Truckee River to lowering base level at Pyramid Lake, Nevada, based on historical air photos and LiDAR data. Geosphere 8, 607–627.
Adams, K.D., Bacon, S.N., Lancaster, N., Rhodes, E.J., Negrini, R.M., 2014. How wet can it get? Defining future climate extremes based on late Holocene lake-level records. Geol. Soc. Am. Abstr. Programs 46, 745.
Bacon, C.R., 1983. Eruptive history of mount Mazama and Crater Lake Caldera, Cascade range, U.S.A. J. Volcanol. Geotherm. Res. 18, 57–115.
Barron, J.A., Anderson, L., 2011. Enhanced Late Holocene ENSO/PDO expression along the margins of the eastern North Pacific. Quat. Int. 235, 3–12.
Barron, J.A., Metcalfe, S.E., Addison, J.A., 2012. Response of the North American monsoon to regional changes in ocean surface temperature. Paleoceanography 27.
Beaty, R.M., Taylor, A.H., 2009. A 14 000 year sedimentary charcoal record of fire from the northern Sierra Nevada, Lake Tahoe Basin, California, USA. Holocene 19, 347–358.
Benson, L., Kashgarian, M., Rye, R., Lund, S., Paillet, F., Smoot, J., Kester, C., Mensing, S., Meko, D., Lindström, S., 2002. Holocene multidecadal and multicentennial droughts affecting Northern California and Nevada. Quat. Sci. Rev. 21, 659–682.
Benson, L.V., Meyers, P.A., Spencer, R., 1991. Change in the size of Walker Lake during the past 5000 years. Palaeogeogr. Palaeoclimatol. Palaeoecol. 81, 189–214.
Berger, A., Loutre, M.-F., 1991. Insolation values for the climate of the last 10 million years. Quat. Sci. Rev. 10, 297–317.
Bowerman, N.D., Clark, D.H., 2011. Holocene glaciation of the central Sierra Nevada, California. Quat. Sci. Rev. 30, 1067–1085.
Bradbury, J.P., Forester, R., Thompson, R., 1990. Late Quaternary Paleolimnology of Walker Lake, Nevada, Paleolimnology and the Reconstruction of Ancient Environments. Springer, pp. 39–57.
Briggs, R.W., Wesnousky, S.G., Adams, K.D., 2005. Late pleistocene and late Holocene lake highstands in the Pyramid Lake subbasin of Lake Lahontan, Nevada, USA. Quat. Res. 64, 257–263.
Bronk Ramsey, C., 2009. Bayesian analysis of radiocarbon dates. Radiocarbon 51, 337–360.
Brothers, D.S., Kent, G.M., Driscoll, N.W., Smith, S.B., Karlin, R., Dingler, J.A., Harding, A.J., Seitz, G.G., Babcock, J.M., 2009. New constraints on deformation, slip rate, and timing of the most recent earthquake on the West Tahoe–Dollar Point Fault, Lake Tahoe Basin, California. Bull. Seismol. Soc. Am. 99, 499–519.
Brown, E., Johnson, T., Scholz, C., Cohen, A., King, J., 2007. Abrupt change in tropical African climate linked to the bipolar seesaw over the past 55,000 years. Geophys. Res. Lett. 34.
Brown, E.T., 2011. Lake Malawi's response to "megadrought" terminations: sedimentary records of flooding, weathering and erosion. Palaeogeogr. Palaeoclimatol. Palaeoecol. 303, 120–125.
Calvert, S., Pedersen, T., Karlin, R., 2001. Geochemical and isotopic evidence for post-glacial palaeoceanographic changes in Saanich Inlet, British Columbia. Mar. Geol. 174, 287–305.
Clark, D.H., Gillespie, A.R., 1997. Timing and significance of late-glacial and Holocene cirque glaciation in the Sierra Nevada, California. Quat. Int. 38, 21–38.
Cohen, A.S., 2003. Paleolimnology: the History and Evolution of Lake Systems. Oxford University Press, USA.
Davis, J.O., 1978. Quaternary Tephrochronology of the Lake Lahontan Area, Nevada and California. University of Nevada.
Dean Jr., W.E., 1974. Determination of carbonate and organic matter in calcareous sediments and sedimentary rocks by loss on ignition: comparison with other methods. J. Sediment. Res. 44.
Dong, S., Ucarkus, G., Wesnousky, S.G., Maloney, J., Kent, G., Driscoll, N., Baskin, R., 2014. Strike-slip faulting along the Wassuk Range of the northern Walker Lane, Nevada. Geosphere 10, 40–48.
Engstrom, D.R., Fitzgerald, W.F., Cooke, C.A., Lamborg, C.H., Drevnick, P.E., Swain, E.B., Balogh, S.J., Balcom, P.H., 2014. Atmospheric Hg emissions from preindustrial gold and silver extraction in the Americas: a reevaluation from lake-sediment archives. Environ. Sci. Technol. 48, 6533–6543.
Goldberg, S., Ball, G., Allen, B., Schladow, S., Simpson, A., Masoom, H., Soong, R., Graven, H., Aluwihare, L., 2015. Refractory dissolved organic nitrogen accumulation in high-elevation lakes. Nat. Commun. 6.
Grayson, D.K., 2011. The Great Basin: a Natural Prehistory. Univ of California Press.
Guyard, H., Chapron, E., St-Onge, G., Anselmetti, F.S., Arnaud, F., Magand, O., Francus, P., Mélières, M.-A., 2007. High-altitude varve records of abrupt environmental changes and mining activity over the last 4000 years in the Western French Alps (Lake Bramant, Grandes Rousses Massif). Quat. Sci. Rev. 26, 2644–2660.
Guyard, H., St-Onge, G., Pienitz, R., Francus, P., Zolitschka, B., Clarke, G.K., Hausmann, S., Salonen, V.-P., Lajeunesse, P., Ledoux, G., 2011. New insights into Late Pleistocene glacial and postglacial history of northernmost Ungava (Canada) from Pingualuit Crater Lake sediments. Quat. Sci. Rev. 30, 3892–3907.
Hanes, T., 1981. Hydrologic analysis of the fallen leaf Lake watershed and operations plan for fallen leaf Lake: US Forest service report. Region 5, 1–44.
Hyne, N.J., Chelminski, P., Gorsline, D.S., Goldman, C.R., 1972. Quaternary history of Lake tahoe, California-Nevada. Geol. Soc. Am. Bull. 83, 1435–1448.
Johnson, B.E., 2013. Anthropogenic and Climatic Influences on the Diatom Flora within the Fallen Leaf Lake Watershed, Lake Tahoe Basin, California. UNIVERSITY OF NEVADA, RENO.
Juggins, S., 2007. C2 Version 1.5: Software for Ecological and Palaeoecological Data Analysis and Visualisation. University of Newcastle, Newcastle upon Tyne.
King, G.Q., 1993. Late quaternary history of the lower Walker river and its implications for the Lahontan paleolake system. Phys. Geogr. 14, 81–96.
Kleppe, J., Brothers, D.S., Kent, G.M., Biondi, F., Jensen, S., Driscoll, N.W., 2011. Duration and severity of Medieval drought in the Lake Tahoe Basin. Quat. Sci. Rev. 30, 3269–3279.
Kleppe, J.A., 2005. A study of ancient trees rooted 36.5 m (120′) below the surface level of Fallen Leaf Lake. J. Nev. Water Resour. Assoc. 1–13.
Kylander, M.E., Ampel, L., Wohlfarth, B., Veres, D., 2011. High-resolution X-ray fluorescence core scanning analysis of Les Echets (France) sedimentary sequence: new insights from chemical proxies. J. Quat. Sci. 26, 109–117.
Lindström, S., 1990. Submerged tree stumps as indicators of mid-Holocene aridity in the Lake Tahoe Basin. J. Calif. Gt. Basin Anthropol. 146–157.
Maloney, J.M., Noble, P.J., Driscoll, N.W., Kent, G.M., Smith, S.B., Schmauder, G.C., Babcock, J.M., Baskin, R.L., Karlin, R., Kell, A.M., 2013. Paleoseismic history of the fallen leaf segment of the West Tahoe–Dollar Point fault reconstructed from slide deposits in the Lake Tahoe Basin, California-Nevada. Geosphere 9, 1065–1090.
Mann, M.E., Zhang, Z., Rutherford, S., Bradley, R.S., Hughes, M.K., Shindell, D., Ammann, C., Faluvegi, G., Ni, F., 2009. Global signatures and dynamical origins of the little ice age and medieval climate anomaly. Science 326, 1256–1260.
Mehringer Jr., P.J., 1985. Late-Quaternary pollen records from the interior Pacific Northwest and northern Great Basin of the United States. Pollen Rec. Late-Quat. North Am. Sediments 167–189.
Mensing, S., Smith, J., Norman, K.B., Allan, M., 2008. Extended drought in the Great Basin of western North America in the last two millennia reconstructed from pollen records. Quat. Int. 188, 79–89.
Mensing, S.A., Benson, L.V., Kashgarian, M., Lund, S., 2004. A Holocene pollen record of persistent droughts from Pyramid Lake, Nevada, USA. Quat. Res. 62, 29–38.
Mensing, S.A., Sharpe, S.E., Tunno, I., Sada, D.W., Thomas, J.M., Starratt, S., Smith, J., 2013. The Late Holocene dry period: multiproxy evidence for an extended drought between 2800 and 1850 cal yr BP across the central Great Basin, USA. Quat. Sci. Rev. 78, 266–282.
Meyers, P.A., 1994. Preservation of elemental and isotopic source identification of sedimentary organic matter. Chem. Geol. 114, 289–302.
Mortlock, R.A., Froelich, P.N., 1989. A simple method for the rapid determination of biogenic opal in pelagic marine sediments. Deep Sea Res. Part A. Oceanogr. Res. Pap. 36, 1415–1426.
Noble, P.J., Chandra, S., Kreamer, D.K., 2013. Dynamics of phytoplankton distribution in relation to stratification and winter precipitation, Fallen Leaf Lake, California. West. North Am. Nat. 73, 302–322.
O'Hara, B.F., 2007. Weather and Climate of the Reno-Carson City-Lake Tahoe Region. Mackay School of Earth Sciences and Engineering. University of Nevada, Reno.
Oksanen, J., Blanchet, F., Kindt, R., Legendre, P., O'Hara, R., Simpson, G., Solymos, P., Stevens, M., Wagner, H., 2013. Vegan: Community Ecology Package. 2013. R Package Version 2.0-7.
Osleger, D.A., Heyvaert, A.C., Stoner, J.S., Verosub, K.L., 2009. Lacustrine turbidites as indicators of Holocene storminess and climate: Lake Tahoe, California and Nevada. J. Paleolimnol. 42, 103–122.
Phillips, F.M., Zreda, M., Plummer, M.A., Elmore, D., Clark, D.H., 2009. Glacial geology and chronology of Bishop Creek and vicinity, eastern Sierra Nevada, California. Geol. Soc. Am. Bull. 121, 1013–1033.
Porinchu, D.F., MacDonald, G.M., 2003. The use and application of freshwater midges (Chironomidae: Insecta: Diptera) in geographical research. Prog. Phys. Geogr. 27, 378–422.
Reimer, P.J., Baillie, M.G., Bard, E., Bayliss, A., Beck, J.W., Bertrand, C.J., Blackwell, P.G., Buck, C.E., Burr, G.S., Cutler, K.B., 2004. IntCal04 Terrestrial Radiocarbon Age Calibration, 0–26 Cal Kyr BP.
Sarna-Wojcicki, A., Lajoie, K., Meyer, C., Adam, D., Rieck, H., 1991. Tephrochronologic correlation of upper Neogene sediments along the Pacific margin, conterminous United States. Quaternary nonglacial geology—Conterminous united states: geological society of america. Geol. N. Am. 2, 117–140.
Saucedo, G.J., Little, J.D., Watkins, S.E., Davis, J.R., Mascorro, M.T., Walker, V.D., Ford, E.W., 2005. Geologic Map of the Lake Tahoe Basin, California and Nevada. State of California, the Resources Agency. Department of Conservation, California Geological Survey.
Smith, S.B., Karlin, R.E., Kent, G.M., Seitz, G.G., Driscoll, N.W., 2013. Holocene subaqueous paleoseismology of Lake Tahoe. Geol. Soc. Am. Bull. 125, 691–708.
Stine, S., 1990. Late holocene fluctuations of Mono Lake, eastern California. Palaeogeogr. Palaeoclimatol. Palaeoecol. 78, 333–381.
Street, J.H., Anderson, R.S., Paytan, A., 2012. An organic geochemical record of Sierra Nevada climate since the LGM from Swamp Lake, Yosemite. Quat. Sci. Rev. 40, 89–106.

Street, J.H., Anderson, R.S., Rosenbauer, R.J., Paytan, A., 2013. n-Alkane evidence for the onset of wetter conditions in the Sierra Nevada, California (USA) at the mid-late Holocene transition,~ 3.0 ka. Quat. Res. 79, 14–23.

Team, R.C., 2012. R: a Language and Environment for Statistical Computing. R Foundation for Statistical Computing, Vienna, Austria, ISBN 3-900051-07-0. http://www.R-project.org.

Thompson, R.S., 1992. Late quaternary environments in ruby Valley, Nevada. Quat. Res. 37, 1–15.

Weltje, G.J., Tjallingii, R., 2008. Calibration of XRF core scanners for quantitative geochemical logging of sediment cores: theory and application. Earth Planet. Sci. Lett. 274, 423–438.

Wigand, P.E., 1987. Diamond Pond, Harney County, Oregon: vegetation history and water table in the eastern Oregon desert. Gt. Basin Nat. 427–458.

Wigand, P.E., Mehringer Jr., P.J., 1985. Pollen and seed analyses. The archaeology of Hidden Cave, Nevada. Anthropol. Pap. Am. Mus. Nat. Hist. 61, 18–124.

Wigand, P.E., Rhode, D., 2002. Great Basin Vegetation History and Aquatic Systems: the Last 150,000 Years. Great Basin Aquatic Systems History, vol. 33. Smithsonian Institution Press, Smithsonian contributions to earth sciences, Washington, DC, USA, pp. 309–367.

Zimmerman, S.R., Pearl, C., Hemming, S.R., Tamulonis, K., Hemming, N.G., Searle, S.Y., 2011. Freshwater control of ice-rafted debris in the last glacial period at Mono Lake, California, USA. Quat. Res. 76, 264–271.